

Emergence of Distortions in High-Dimensional Guided Diffusion Models

Enrico Ventura^{1,2} Beatrice Achilli¹ Luca Ambrogioni³ Carlo Lucibello^{1,2}

Abstract

Classifier-free guidance (CFG) is the de facto standard for conditional sampling in diffusion models, yet it often leads to a loss of diversity in generated samples. We formalize this phenomenon as generative distortion, defined as the mismatch between the CFG-induced sampling distribution and the true conditional distribution. Considering Gaussian mixtures and their exact scores, and leveraging tools from statistical physics, we characterize the onset of distortion in a high-dimensional regime as a function of the number of classes. Our analysis reveals that distortions emerge through a phase transition in the effective potential governing the guided dynamics. In particular, our dynamical mean-field analysis shows that distortion persists when the number of modes grows exponentially with dimension, but vanishes in the sub-exponential regime. Consistent with prior finite-dimensional results, we further demonstrate that vanilla CFG shifts the mean and shrinks the variance of the conditional distribution. We show that standard CFG schedules are fundamentally incapable of preventing variance shrinkage. Finally, we propose a theoretically motivated guidance schedule featuring a negative-guidance window, which mitigates loss of diversity while preserving class separability.

1. Introduction

Generative diffusion models (Sohl-Dickstein et al., 2015) are undoubtedly the most employed tools for generating images (Ho et al., 2020; Song & Ermon, 2019; Yang et al., 2021) and videos (Ho et al., 2022; Singer et al., 2022; Blattmann et al., 2023). Diffusion models (DMs) synthesize images through a stochastic dynamical denoising process (Sohl-Dickstein et al., 2015). While unconditional diffusion

¹Department of Computing Sciences, Bocconi University, Milan, Italy ²Bocconi Institute for Data Science and Analytics

³Donders Institute for Brain, Cognition and Behaviour, Radboud University, Nijmegen, Netherlands. Correspondence to: Enrico Ventura <enrico.ventura@unibocconi.it>.

Preprint. February 11, 2026.

models already achieve remarkable sample quality, most practical applications require controllable generation, where samples are drawn from a conditional distribution specified by auxiliary information such as class labels or prompts. The consolidated, yet still unclear, ineffectiveness of direct use of trained conditional score (Bradley & Nakkiran, 2025; Rombach et al., 2022) motivated the adoption of guidance mechanisms to amplify the conditioning signal. Classifier-free guidance (CFG) has emerged as the standard approach for conditional sampling in diffusion models, due to its simplicity and empirical effectiveness (Ho & Salimans, 2022; Jiao et al., 2025). By interpolating between unconditional and conditional score functions, CFG allows practitioners to control the strength of conditioning through a single parameter. Increasing this parameter typically improves class separability and alignment with the conditioning signal, but often induces a noticeable loss of diversity in the generated samples (Chidambaram et al., 2024; Ho & Salimans, 2022; Pavasovich et al., 2025). Despite its widespread use, a principled understanding of how CFG modifies the target conditional distribution is still missing. In particular, it remains unclear whether the observed loss of sample diversity is an intrinsic property of guided diffusion dynamics in high dimensions, with recent work suggesting that in some settings, guidance-induced distortions are an intrinsically finite-dimensional effect (Pavasovich et al., 2025). In this work, we address this question by characterizing the notion of generative distortion in large dimensions and for a large number of classes and predicting how CFG, both in its vanilla version and the time-modulated one, tends to transform the conditional distribution of the data.

Related Works

While early empirical analysis has highlighted that higher CFG improves alignment but reduces diversity and overall perceptual quality (Ho & Salimans, 2022; Saharia et al., 2022), later work has tried to overcome such distortions by curbing spatial non-uniformity (Shen et al., 2024), including negative-prompt interactions (Ban et al., 2024; Koulischer et al., 2025), as well as proposing over-saturation artifacts (Sadat et al., 2025) and off-manifold drift (Chung et al., 2025).

Analytical work has studied how guidance reshapes the effective sampling distribution using tractable targets. Fu et al.

(2024) provide a general approach by approximating the guided score from statistical bounds, on the line of Chen et al. (2022). A closed-form analysis of a single-Gaussian model in (Li et al., 2025) has described how guidance shifts means and modifies covariance. Other works (Wu et al., 2024; Bradley & Nakkiran, 2025; Jin et al., 2025b; Chidambaram et al., 2024; Pavasovich et al., 2025; Li & Jiao, 2025) have focused on mixtures of Gaussians and characterized how the data modes get deformed by guidance at different layers of complexity. In this mixture of Gaussian set-up, it is known that class separation is demarcated by symmetry-breaking speciation events, corresponding to branching in the unconditional trajectories (Raya & Ambrogioni, 2023; Biroli et al., 2024). In this context, Jin et al. (2025a) and Pavasovich et al. (2025) investigated the diffusion dynamics under CFG, and provided a coherent three-phase description of guided backward diffusion: the former considers a target where each class is a cluster of modes, characterizing the killing of weaker modes by CFG; the latter proves that, when the target is a high-dimensional mixture of two Gaussians, CFG aligns with conditional diffusion. In fact, Pavasovich et al. (2025) claim that previous studies on mixture of Gaussians might have been biased by the choice of a low-dimensional framework, while CFG, in practice, exploits the blessing of dimensionality to perform well.

In order to avoid destructive distortions, practitioners have designed ways to modulate the guidance level along the backward process (Wang et al., 2024). Motivated by their models, both Pavasovich et al. (2025) and Jin et al. (2025a) have proposed a prescription consisting into applying a low guidance level at early and late times while increasing it in the middle of the process: experimental evidence shows that this procedure saves class separability while tempering the natural variance-shrinkage.

Our contributions

We present some experiments showing generative distortions caused by CFG in experiments with real datasets and architectures. Then, we devise a synthetic setting where the data and conditioning are jointly Gaussian or given by a Gaussian mixture. The unconditional and conditional score functions used in the guided process are taken to be the true ones, with the goal of characterizing the intrinsic bias of CFG, independently of neural approximation errors. Under precise conditions, distortion effects are present also even in high-dimensions, contrary to the setting of Pavasovich et al. (2025). Our analysis displays that:

- (i) Classifier-free guided DMs systematically distort the conditional target whenever the conditioning classes are not well separated.

- (ii) Classifier-free guided DMs always deform the conditional target distribution when the number of classes is exponential in the dimension of the ambient space d , and $d \gg 1$ (a regime possibly approached in text-to-image modeling). This is due to diffusive trajectories being driven by the guided score function during most of the backward process. On the other hand, CFG never deforms the conditional distribution when the number of classes is sub-exponential, since DMs are mostly never effectively guided during the process. This result generalizes Pavasovich et al. (2025) and discards the belief that, for highly multi-modal datasets, CFG aligns with the true conditional distribution in high dimensions.
- (iii) Vanilla CFG and standard CFG time-dependent prescriptions expand the mean and contract the variance of the conditional target distribution.
- (iv) We introduce and analyze CFG strategies, in which the guidance level is progressively decreased and eventually allowed to take negative values. This regime enables the simultaneous expansion of both the mean and the variance of the conditional target distribution, and can be shown, within this theoretical setting, to restore diversity in the generated samples.

2. Generative Diffusion and Classifier-free Guidance (CFG)

2.1. Diffusion Models

In this paper, we will consider a variance-exploding (Song et al., 2021) forward process where the data $\mathbf{x}_0 \sim p_0(\mathbf{x})$ evolves according to the equation

$$d\mathbf{x}_t = d\mathbf{W}_t, \quad (1)$$

where $d\mathbf{W}_t$ is standard Brownian motion in dimension d . Solution of Eq. (1) have marginal density

$$p_t(\mathbf{x}_t) = \mathbb{E}_{\mathbf{x}_0 \sim p_0} \left[\frac{1}{(2\pi t)^{d/2}} e^{-\frac{\|\mathbf{x}_t - \mathbf{x}_0\|^2}{2t}} \right]. \quad (2)$$

The *target distribution* $p_0(\mathbf{x})$ is then recovered by reversing the diffusion process (Anderson, 1982). We initialize this reverse (or *backward*) process from $\mathbf{x}_T \sim \mathcal{N}(0, T \cdot I_d)$ at some large time T . The SDE running back in time used for generation reads

$$d\mathbf{x}_t = -s_t(\mathbf{x}_t)dt + d\mathbf{W}_t, \quad (3)$$

where $s_t(\mathbf{x}_t) = \nabla_{\mathbf{x}} \log p_t(\mathbf{x}_t)$ is called *score function*. From a set of training points $\{\mathbf{y}^1, \dots, \mathbf{y}^N\} \stackrel{\text{iid}}{\sim} p_0$, we can train a neural approximation of $s_t(\mathbf{x}_t)$ using the denoising score matching objective (Hyvärinen & Dayan, 2005; Vincent, 2011; Ho et al., 2020).

2.2. Classifier-free Guidance (CFG)

A crucial need for DM users is to sample conditionally on a given context, e.g. a text prompt for text-to-image generation. The most direct option is to train a model to fit the conditional score function $\nabla_{\mathbf{x}} \log p_t(\mathbf{x}_t|\mathbf{c})$ and run through that the reverse process. Neural approximations though, especially in the presence of a large conditioning space, often provide weak estimations and yield poor adherence to the conditioning and low quality samples. This motivated the use of *guidance* methods that bias sampling toward higher conditional likelihood (Bradley & Nakkiran, 2025; Ho & Salimans, 2022). Early work used *classifier guidance* (Dhariwal & Nichol, 2021), adding the gradient of a noise-conditioned classifier $\nabla_{\mathbf{x}} \log p_{\phi}(\mathbf{c}|\mathbf{x}_t)$ to the vanilla diffusion score to steer samples. While effective, it requires a separate classifier and extra backpropagation at every step, increasing compute and making results sensitive to classifier errors and artifacts at high guidance strength. Practitioners have then found the way to re-express the classifier score $\nabla_{\mathbf{x}} \log p_t(\mathbf{x}_t|\mathbf{c})$ in terms of the original conditional score function $p_t(\mathbf{x}_t|\mathbf{c})$ which involves no external classifier and labeling pre-process. They hence introduced a novel drift function that reads

$$\tilde{s}_t(\mathbf{x}_t|\mathbf{c}) = (1+w)\nabla_{\mathbf{x}} \log p_t(\mathbf{x}_t|\mathbf{c}) - w\nabla_{\mathbf{x}} \log p_t(\mathbf{x}_t), \quad (4)$$

where the *guidance level* w controls the degree of conditioning: $w = -1$ reproduces unconditional diffusion, $w = 0$ reproduces conditional diffusion with no guidance, $w > 0$ reinforces conditioning. This method is called Classifier-free Guidance (CFG) for generative diffusion (Ho & Salimans, 2022).

3. Measuring Distortion in Real Datasets

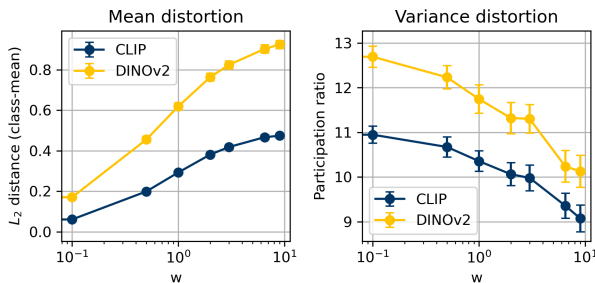


Figure 1. Measures of distortion from a guided Stable Diffusion (v1.5) model, in feature space, as a function of the guidance level w , averaged over 100 samples. Blue circles refer to CLIP feature extractor, yellow ones to DINOv2. Left: Quadratic distance between the mean across the features at a given guidance level and the one measured at $w = 0$. The increasing distance signals a gain in class separability. Right: Participation ratio of the eigenvalues of the empirical covariance matrix across samples showing a loss of sample diversity with increasing guidance.

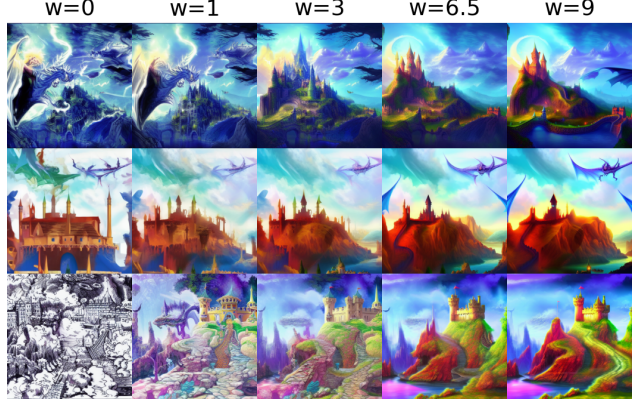


Figure 2. Samples generated for the prompt *a fantasy landscape with castles and dragons, vibrant colors, digital art* with Stable Diffusion v1.5. Rows are different random seeds, columns refer to guidance levels.

We analyze the effect of CFG on image variability using a dataset of images generated from Stable Diffusion v1.5 (Rombach et al., 2022). We select 50 prompts, and for each input prompt p , we generate 20 images at different guidance levels. For each image, we extract the corresponding features f by means of CLIP and DINOv2 extractors. For each prompt and guidance level, we measure two quantities: i) mean distortion $\mathbb{E}_p \text{ MSE}(\bar{f}_{p,w}, \bar{f}_{p,0})$ with $\bar{f}_{p,w} = \mathbb{E}_{f|w,p} f$, and ii) participation ratio $\text{PR}_w = \mathbb{E}_p \left[\frac{(\sum_i \lambda_i^{p,w})^2}{\sum_i (\lambda_i^{p,w})^2} \right]$, where $\lambda_i^{p,w}$ are PCA eigenvalues of the features for each prompt and guidance level. The first observable quantifies the deviation of the guided mean with respect to the conditional one; the second quantity measures the shrinkage of the sampling distribution, hence the loss of diversity. Results are reported in Figure 1. The mean distortion increases with w , signaling an expansion of the mean and a gain in class separability; the participation ratio decreases with w , signaling a loss in diversity, i.e. generated images tend to look similar when guidance gets strong. This trend is what, in principle, we would like to characterize analytically and mitigate, or revert, by means of a scheduling strategy. The systematic loss of diversity is noticeable in Figure 2, which presents generated images for one prompt at different guidance levels.

4. Generative distortion in CFG

Now we give quantitative insights in two simple synthetic setups about the deformation effects of CFG. We are interested in computing the deviation of the distribution $\tilde{p}_0(\mathbf{x}|\mathbf{c})$ induced by CFG from the true target distribution $p_0(\mathbf{x}|\mathbf{c})$, assuming that we have access to the true scores to derive the CFG score in (4)

In Section 4.1 the classes are continuous and jointly Gaussian distributed with the data. The CFG sampling process

can be exactly integrated and we can analytically quantify the distortion. When submitting this manuscript, we realized that [Li et al. \(2025\)](#) had performed a similar analysis of the same conditional distribution in concurrence with this work, obtaining related results.

In Section 4.2, the data distribution will be a mixture of M Gaussians, with each component being a class. We analyze three different scaling regimes of M with respect to d , and quantify the distortion in the limit $d \rightarrow \infty$. We approximately describe the dynamical potential by means of an effective Random Energy model (REM) ([Derrida, 1981](#); [Lucibello & Mézard, 2024](#)) that undergoes collapse and condensation phase transitions ([Biroli et al., 2024](#); [Biroli & Mézard, 2023](#); [Achilli et al., 2025](#)).

4.1. Continuous Classes

We consider a joint multivariate Gaussian target distribution over $(\mathbf{c}, \mathbf{x}) \in \mathbb{R}^{d_1} \times \mathbb{R}^{d_2}$, specifically

$$p_0(\mathbf{c}, \mathbf{x}) = \mathcal{N}\left(\begin{pmatrix} \mathbf{c} \\ \mathbf{x} \end{pmatrix}; \mathbf{0}, \Sigma\right), \quad \Sigma = \begin{pmatrix} \Sigma_{cc} & \Sigma_{cx} \\ \Sigma_{xc} & \Sigma_{xx} \end{pmatrix}, \quad (5)$$

where $\mathbf{c} \in \mathbb{R}^{d_1}$ and $\mathbf{x} \in \mathbb{R}^{d_2}$, with $d_1 + d_2 = d$ and $\Sigma_{xc} = \Sigma_{cx}^\top$. Let us pin the set of features \mathbf{c} , as it were our *class*, and consider a variance-exploding forward process in the subspace relative to \mathbf{x} , namely

$$\mathbf{x}_0 \sim p_0, \quad \mathbf{x}_t = \mathbf{x}_0 + \sqrt{t} \boldsymbol{\epsilon}_t, \quad \boldsymbol{\epsilon}_t \sim \mathcal{N}(0, I_d). \quad (6)$$

Then we have

$$p_t(\mathbf{x}_t | \mathbf{c}) = \mathcal{N}(\mathbf{x}_t; \boldsymbol{\mu}, \Sigma_{x|c}(t)), \quad (7)$$

$$p_t(\mathbf{x}_t) = \mathcal{N}(\mathbf{x}_t; \mathbf{0}, \Sigma_{xx}(t)), \quad (8)$$

with $\boldsymbol{\mu} = \Sigma_{xc}\Sigma_{cc}^{-1}\mathbf{c}$, $\Sigma_{xx}(t) = \Sigma_{xx} + tI_{d_2}$, $\Sigma_{x|c}(t) = \Sigma_{x|c} + tI_{d_2}$ and $\Sigma_{x|c} = \Sigma_{xx} - \Sigma_{xc}\Sigma_{cc}^{-1}\Sigma_{cx}$. The guided score can now be obtained by substituting the corresponding conditional and true score functions into the formula in Eq. (4). The CFG distribution $\tilde{p}_t(\mathbf{x}_t | \mathbf{c})$ is obtained integrating back in time the SDE

$$d\mathbf{x}_t = -A(t)\mathbf{x}_t dt - B(t)\boldsymbol{\mu} dt + d\mathbf{W}_t, \quad (9)$$

where

$$A(t) = -(1+w)(\Sigma_{x|c}(t))^{-1} + w(\Sigma_{xx}(t))^{-1}, \quad (10)$$

$$B(t) = (1+w)(\Sigma_{x|c}(t))^{-1}. \quad (11)$$

Let us assume that matrices Σ_{xx} and $\Sigma_{x|c}$ commute by construction and that they share a basis of eigenvectors $\{\mathbf{v}^{(i)}\}_{i=1}^{d_2}$. Then we are able to integrate the SDE (see Appendix A). We conclude that the marginal density is Gaussian with mean given by

$$\boldsymbol{\mu}_w(t) = \sum_{i=1}^{d_2} \lambda_i(t) (\mathbf{v}^{(i),\top} \boldsymbol{\mu}) \mathbf{v}^{(i)}, \quad (12)$$

with coefficients

$$\lambda_i(t) = \begin{cases} \frac{1}{(s_i - r_i)} \left[\frac{(s_i + t)^{w+1}}{(r_i + t)^w} - (r_i + t) \right], & s_i \neq r_i, \\ 1 + w & s_i = r_i. \end{cases} \quad (13)$$

where $\{r_i, s_i\}_{i=1}^{d_2}$ are, respectively, the eigenvalues of the matrices Σ_{xx} and $\Sigma_{x|c}$.

The covariance matrix of the same distribution is given by

$$\Sigma_w(t) = \sum_{i=1}^{d_2} \Lambda_i(t)(s_i + t) \mathbf{v}^{(i)} \mathbf{v}^{(i),\top}, \quad (14)$$

with coefficients

$$\Lambda_i(t) = \begin{cases} \frac{1}{(2w+1)(s_i - r_i)} \left[\frac{(s_i + t)^{1+2w}}{(r_i + t)^{2w}} - (r_i + t) \right], & \text{if } s_i \neq r_i, \\ 1 & \text{if } s_i = r_i. \end{cases} \quad (15)$$

The behavior of λ and Λ at $t = 0$ is reported in Figure 3 as a function of the ratio s/r , which is handy since $r_i \geq s_i \forall i$ by construction. As one can notice, $\lambda_i \geq 1$ and $\Lambda_i \leq 1 \forall i$. Now, in order to compare $\boldsymbol{\mu}_w$ at time $t = 0$ with the undistorted mean $\boldsymbol{\mu}$, let us express the latter in terms of the eigen-basis $\{\mathbf{v}^{(i)}\}_{i=1}^{d_2}$ as

$$\boldsymbol{\mu} = \sum_{i=1}^{d_2} (\mathbf{v}^{(i),\top} \boldsymbol{\mu}) \mathbf{v}^{(i)}. \quad (16)$$

Since $\lambda_i \geq 1$, we can conclude that the mean $\boldsymbol{\mu}$ is always expanded by CFG for this class of target densities. Similarly, for the second moments, let us express the conditional covariance matrix through its spectral decomposition

$$\Sigma_{x|c} = \sum_{i=1}^{d_2} s_i \mathbf{v}^{(i)} \mathbf{v}^{(i),\top}. \quad (17)$$

Since $\Lambda_i \leq 1 \forall i$, we conclude that the conditional covariance matrix $\Sigma_{x|c}$ is always contracted by CFG. Let us stress that the derivations above do not depend on the entity of the dimension d itself. Figure 4 reports the norm of mean and covariance matrix, showing increasing distortion with w .

4.2. Separated Classes: Mixtures of M Gaussians

We now consider the full target distribution

$$p_0(\mathbf{x}) = \frac{1}{M} \sum_{\mu=1}^M \mathcal{N}(\mathbf{x}; \mathbf{c}^\mu, \sigma^2), \quad \mathbf{c}^\mu \sim \mathcal{N}(0, I_d), \quad (18)$$

that is an homogeneous mixture of M Gaussians in a d dimensional real space. In this setup, we are performing CFG by conditioning the process with respect to one class coinciding with one of the modes of the mixture. Specifically we choose $\mathbf{c} \equiv \mathbf{c}^1$, with $p_0(\mathbf{x} | \mathbf{c}^1) = \mathcal{N}(\mathbf{x}; \mathbf{c}^1, \sigma^2)$.

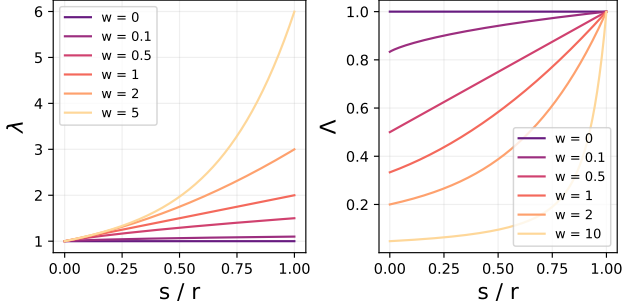


Figure 3. The coefficients λ and Λ governing the distortion of CFG in the Gaussian setting, at $t = 0$ and as a function of w and the ratio s/r , where (s, r) are eigenvalues, respectively, of $\Sigma_{x|c}$ and Σ_{xx} . Since $\lambda \geq 1$, the mean of the conditional target distribution is always expanded, while $\Lambda \leq 1$ implies a systematic contraction of the covariance matrix.

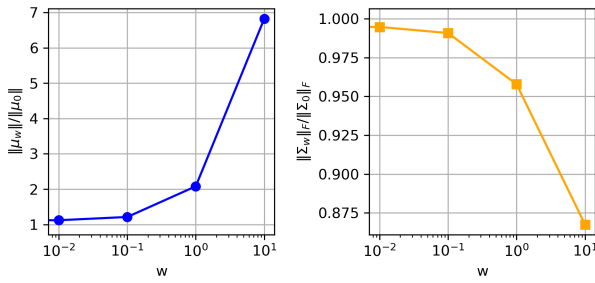


Figure 4. Measure of distortion from numerical simulations for CFG on jointly Gaussian classes and data, showing increased class separation and decreased diversity with increasing w . Dimensions are $d_1 = 1$, $d_2 = 9$. Left: the norm of the CFG mean divided by the true conditional mean. Right: Frobenius norm of Σ_w divided by the true conditional covariance matrix.

The evolving sampling distributions along a variance-exploding forward process, as presented in Section 4.1, read

$$p_t(\mathbf{x}_t) = \frac{1}{M} \sum_{\mu=1}^M \mathcal{N}(\mathbf{x}_t; \mathbf{c}^\mu, \sigma^2 + t), \quad (19)$$

$$p_t(\mathbf{x}_t | \mathbf{c}^1) = \mathcal{N}(\mathbf{x}_t; \mathbf{c}^1, \sigma^2 + t). \quad (20)$$

Our goal consists again in finding the probability distribution $\tilde{p}_t(\mathbf{x}_t | \mathbf{c}^1)$ induced by the CFG process. For convenience of analysis, we rewrite the time-reversed SDE as

$$d\mathbf{x}_t = \nabla_{\mathbf{x}} V_{\text{eff}}(\mathbf{x}_t) dt + d\mathbf{W}_t. \quad (21)$$

where we defined the effective time-dependent potential

$$V_{\text{eff}}(\mathbf{x}_t) = -\log \left[\frac{p_t(\mathbf{x}_t | \mathbf{c}^1)^{1+w}}{p_t(\mathbf{x}_t)^w} \right] \quad (22)$$

$$= V_{\text{cond}}(\mathbf{x}_t) + V_{\text{guided}}(\mathbf{x}_t) \quad (23)$$

The potential has been decomposed into the pure conditional

part

$$V_{\text{cond}}(\mathbf{x}_t) = \frac{1}{2} \frac{\|\mathbf{x}_t - \mathbf{c}^1\|^2}{\sigma^2 + t} + \frac{d}{2} \log(2\pi t), \quad (24)$$

that is a quadratic potential centered on \mathbf{c}^1 which does not depend on w , and a guiding term

$$V_{\text{guided}}(\mathbf{x}_t) = -w \cdot \log(M) + w \log \left(1 + \sum_{\mu>1}^M e^{-\frac{1}{2(\sigma^2+t)} (\|\mathbf{x}_t - \mathbf{c}^\mu\|^2 - \|\mathbf{x}_t - \mathbf{c}^1\|^2)} \right), \quad (25)$$

that depends linearly on w and also on the non-conditioning classes $\{\mathbf{c}^\mu\}_{\mu>1}$.

4.2.1. SIMPLIFIED DYNAMICAL MEAN FIELD THEORY

Inspired by Pavasovich et al. (2025), we analyze the effective diffusion potential through the lens of statistical physics. We will use a simplified *dynamical mean-field* description, replacing $V_{\text{guided}}(\mathbf{x}_t)$ with $\mathbb{E}V_{\text{guided}}(\mathbf{x}_t)$ where expectation is over the realization of all \mathbf{c}^μ except for the reference one \mathbf{c}^1 .

We consider different scaling regimes of M with respect to the ambient space dimensions d . Let the number of centroids be $M = e^{\beta(d) \cdot d}$, where $\beta(d)$ will be further specified later. By assuming $d \gg 1$, the approximated guided potential can be written as

$$V_{\text{guided}}(\mathbf{x}_t) \approx -w \left[d\beta(d) - \log \left(1 + e^{d\phi_t(\mathbf{x}_t | \mathbf{c}^1)} \right) \right], \quad (26)$$

where $\phi_t(\mathbf{x}_t | \mathbf{c}^1)$ is the free energy of a Random Energy Model (REM), a celebrated statistical physics model that has already been used in the analysis of DMs (Biroli et al., 2024; Achilli et al., 2025; 2024; George et al., 2025). Explicit calculation of ϕ_t is given in Appendix B. Depending on the choice of $\beta(d)$, σ^2 , and the value of the diffusion time t , the potential V_{eff} can assume two different quadratic shapes that drive the backward process.

When $\phi_t(\mathbf{x}_t | \mathbf{c}^1) > 0$, which we call *guided phase*, we have

$$V_{\text{eff}}(\mathbf{x}_t) = \frac{(1+w)}{2} \frac{\|\mathbf{x}_t - \mathbf{c}^1\|^2}{\sigma^2 + t} - \frac{w\|\mathbf{x}_t\|^2}{2(\sigma^2 + t + 1)} + \frac{dw}{2} \log \left(1 + \frac{1}{\sigma^2 + t} \right) + \frac{d}{2} \log(2\pi t), \quad (27)$$

If $\phi_t(\mathbf{x}_t | \mathbf{c}^1) \leq 0$ instead, the system is in the *conditional phase*, with a steady minimum corresponding to the class \mathbf{c}^1 itself:

$$V_{\text{eff}}(\mathbf{x}_t) = \frac{1}{2} \frac{\|\mathbf{x}_t - \mathbf{c}^1\|^2}{\sigma^2 + t} + \frac{d}{2} \log(2\pi t) - dw\beta(d). \quad (28)$$

Once the expressions for V_{eff} and its gradient $\nabla_{\mathbf{x}}V_{\text{eff}}$ is obtained, we can solve the CFG SDE in Eq. (21) piecewise integrating the different phases. The integration can be performed analytically thanks to the piecewise quadratic nature of $V_{\text{eff}}(\mathbf{x})$. The transition between the two phases of the potential is obtained when the free-energy changes sign. We name the time at which such transition takes place *speciation time* t_s , in continuation with the literature (Biroli et al., 2024). We find t_s by solving the following implicit equation

$$\lim_{d \rightarrow \infty} [\beta(d) + \zeta_{t_s}(\sigma^2, w)] = 0, \quad (29)$$

where ζ_t is the moment generating function of the REM and is defined in the Appendix. By taking into account that, at $t = t_s$, the system lives in the guided phase and by substituting the correct trajectory \mathbf{x}_t into Eq. (29) we find that ζ_t decreases monotonically in time and $\zeta_t(w) = -\frac{(1+w)}{t} + \mathcal{O}(\frac{1}{t^2})$ at large times t . This implies that, if the number of classes is sub-exponential, the speciation time diverges as

$$t_s(w, d) = \mathcal{O}\left(\frac{1+w}{\beta(d)}\right), \quad (30)$$

while $\beta(d)$ is vanishing with d . Otherwise, if the number of centroids is exponential in d , then $t_s = \mathcal{O}(1)$ can be derived by solving the transition condition, and it will depend on the whole set of parameters w , β , and σ^2 . Once the speciation time t_s is computed, it can be used as the initial condition for the backward SDE inside the conditional phase, while the guided phase will be integrated starting from a diverging horizon time $T \rightarrow \infty$, as detailed in Appendix C.4. We thus obtain the statistics for the diffusive trajectory down to $t = 0$ and measure how $\tilde{p}_0(\mathbf{x}_0|\mathbf{c}^1)$ deviates from $p_0(\mathbf{x}_0|\mathbf{c}^1)$. Specifically, we can measure the following two distortion estimators

$$\delta_\mu = \lim_{d \rightarrow \infty} \frac{\mathbf{c}^1 \cdot (\boldsymbol{\mu}_w(0) - \mathbf{c}^1)}{d}, \quad (31)$$

$$\delta_{\sigma^2} = \frac{\sigma_w^2(0) - \sigma^2}{\sigma^2}. \quad (32)$$

The first estimator measures how the *guided mean* $\boldsymbol{\mu}_w(t = 0)$ is shifted with respect to the conditional mean, i.e. the class \mathbf{c}^1 itself. The second estimator quantifies how the *guided variance* $\sigma_w^2(t = 0)$ is deviating from the variance σ^2 of the conditional distribution.

4.2.2. EXPONENTIAL NUMBER OF CLASSES

Let us first evaluate mixtures of Gaussians with $M = e^{\beta d}$ with β a tunable parameter that does not depend on $d \gg 1$. As shown in Section 4.2.1, the speciation time in this regime is finite. This aspect of CFG is the main responsible for the deformation of the target distribution in CFG: the absence of the transition to the conditional phase, or a finite speciation time t_s , implies distortion; on the other hand, a value

of t_s that diverges with d implies a negligible distortion effect. The heuristics behind the phenomenology lies in the nature of the backward SDE and the fact that we integrate the process inside the conditional phase starting from t_s : if initialization is far away from sampling time, the system has all the time to converge to the right target distribution, for $t < t_s$; conversely, if t_s is close to sampling time, i.e. $t_s = \mathcal{O}(1)$, the conditional target distribution is not correctly recovered; there might be also the case where $t_s < 0$, implying the transition to the conditional phase to never occur: in this case we can only have distortion. This correspondence between the magnitude of t_s and distortion effects can be well appreciated from Figure 5, that reports t_s and the distortion estimators $\delta_\mu, \delta_{\sigma^2}$ for different realizations of parameters β and w for a fixed $\sigma^2 = 0.5$. Similarly, Figure 6 displays the behavior of distortion estimators as functions of w at fixed values of σ^2 and β . As one can notice, these observables are not monotonic with respect to the guidance level. Instead, δ_μ shows a maximum and δ_{σ^2} a minimum in w . This effect is caused by the fact that, as evident from the complementary Figure 10 in Appendix C.4, speciation time t_s generally increases with w . Moreover, Figure 6 reports measurements from numerical simulations of the guided diffusion, showing close agreement with the simplified dynamical mean-field predictions.

4.2.3. SUB-EXPONENTIAL NUMBER OF CLASSES

Examples of sub-exponential scaling regimes of M are: the *polynomial* regime where $M = N^a$ with $a > 1$, so that $\beta = \mathcal{O}\left(\frac{\log d}{d}\right)$; the *finite classes* regime where $M = \mathcal{O}(1)$ and $\beta = \mathcal{O}\left(\frac{1}{d}\right)$. As shown in Section 4.2.1, these regimes are not affected by CFG since the speciation time diverges with d . As a consequence, the sampling distribution must align with the conditional data distribution at $t = 0$. The same result was derived by Pavasovich et al. (2025) for a mixture of two well-separated Gaussians.

5. Evaluating CFG strategies

The goal of CFG is to increase the quality of samples and adherence to the conditioning. As already observed, both empirically and theoretically, this procedure might induce a loss of diversity with respect to the true conditional distribution. In our analysis, for both the joint Gaussian model with continuous classes and the mixture of Gaussians model, this effect is associated with a contraction of the second cumulant of the samples' distribution. Building on our theory, the goal of this Section is to analyze the effects of CFG scheduling, that is, introducing a dependence on w on diffusion time, and to propose a novel procedure that boosts class separation while avoiding loss of diversity. We present here in the main text an analysis based on the mixture of Gaussians with an exponential number of classes. We also

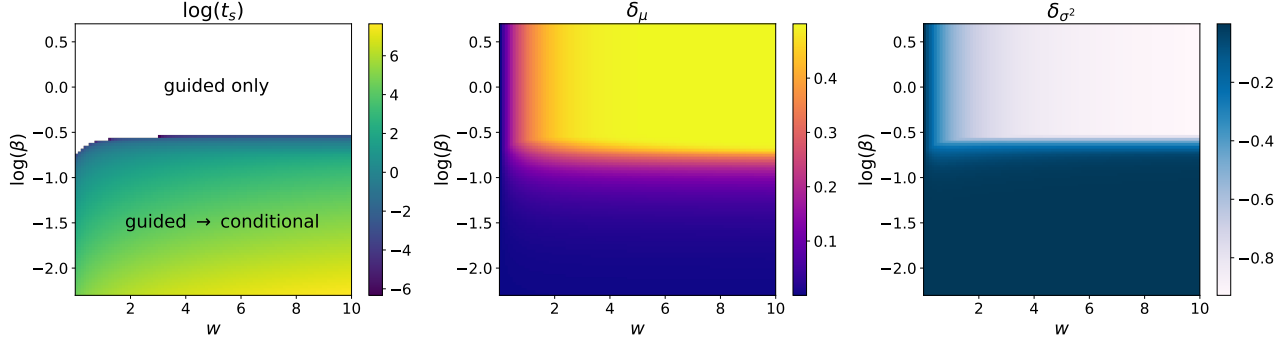


Figure 5. Speciation time t_s and the distortion estimators in the exponential regime predicted by the theory as functions of the control parameters $\beta = \log(M)/d$ and w , for $\sigma^2 = 0.5$. In the white region, there is no speciation and therefore we have no transition to the conditional phase. This regime displays strong distortion in the conditional sampling as testified by the behavior of δ_μ and δ_{σ^2} . In the small β regime instead, where the transition occurs, distortion is weak.

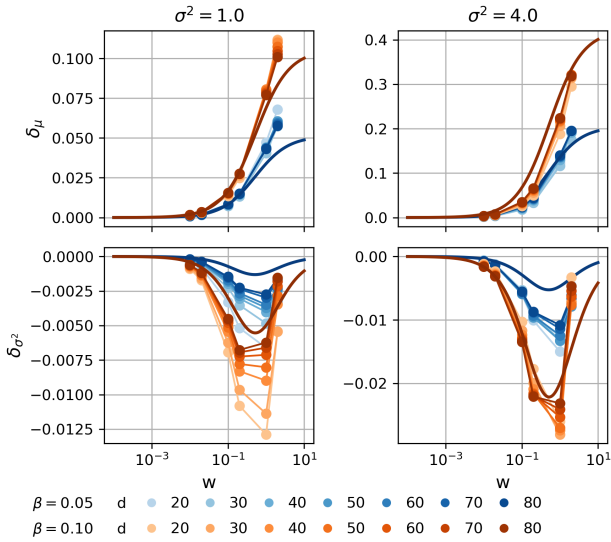


Figure 6. Comparison of the simplified dynamical mean-field theory prediction (full lines) with numerical simulations of CFG (circles) for a mixture of an exponential number of Gaussians target distribution. The plots show The distortion estimators δ_μ and δ_{σ^2} . The theory matches qualitatively and also quantitatively the numerics at increasing d .

performed a similar analysis in the case of the joint Gaussian with continuous classes, reported in Appendix D.2, that shows consistent results.

5.1. The sign of w drives distortion

Let us now provide a heuristic argument that leads to a new CFG prescription hindering accidental loss of diversity due to guidance.

When the target data distribution is a mixture of Gaussians, the potential in the *guided phase*, is a quadratic form: $V_{\text{eff}}(\mathbf{x}_t) = \frac{\|\mathbf{x}_t - \mathbf{c}_t^*\|^2}{2\sigma_t^{*2}} + \text{others}$. The bottom of the potential

well is a moving target, chased by the diffusive process, that reads

$$\mathbf{c}_t^* = \frac{(1+w)(\sigma^2 + t + 1)}{w + \sigma^2 + t + 1} \mathbf{c}^1. \quad (33)$$

If we compare this position with \mathbf{c}^1 we realize that $\|\mathbf{c}_t^*\| > \|\mathbf{c}^1\|$, if $w > 0$. This observation suggests that positive guidance levels tend to drive $\mu_w(t)$ to be larger in magnitude than the class. Similarly, the typical width of the well reads

$$\sigma_t^{*2} = \frac{(\sigma^2 + t)(\sigma^2 + t + 1)}{\sigma^2 + t + 1 + w}. \quad (34)$$

By comparing this width with the variance of the conditional distribution, i.e. $\sigma^2 + t$, we conclude that $\sigma_t^{*2} < \sigma^2 + t$, if $w > 0$, implying that a positive guidance level is driving $\sigma_w^2(t)$ to become smaller than σ^2 at small times. Based on this observation, we want to design a CFG strategy that reaches the following two objectives: class *separation*, i.e. $\delta_\mu > 0$: this effect must be induced by exposing the guided trajectory to a *positive* guidance level; sample *diversity*, i.e. $\delta_{\sigma^2} \geq 0$: this effect must be induced by exposing the guided trajectory to a *negative* guidance level.

5.2. Increasing Diversity through a negative Guidance window

We hence propose an “early-high” CFG schedule that includes a time window of tunable width where the guidance level is set to negative values. An early-high schedule starts the backward process with a high value of w , and decreases it progressively (Wang et al., 2024; Jin et al., 2025a). The simplest prescription that we can study in our theoretical framework reads

$$w(t) = w_0 + \omega \cdot t, \quad w_0 \geq -1, \quad \omega > 0. \quad (35)$$

In this procedure, the trajectory is exposed to two different signs of the guidance level across the backward process: at large times (start of the process), the guided diffusive

trajectory is pushed to expand the means and contract the variances; when $0 < t < \max(0, -\frac{w_0}{\omega})$, the system is induced to reduce means and expand variances.

By substituting $w(t)$ into the backward SDE in Eq. (21) we obtain the typical guided trajectories, their statistics and a pair of distortion estimators δ_μ and δ_{σ^2} . Detailed calculations are reported in Appendix D.3. For simplicity, we consider β large enough that the dynamics stays in the *guided-only* phase. We fix $\sigma^2 = 0.75$ and $\beta \gg 1$ and vary w_0 and ω to construct the phase diagram depicted in Figure 7. We identify a region in the phase diagram where $\delta_\mu > 0$ and $\delta_{\sigma^2} > 0$, which lies in the $w_0 < 0$ half-plane, as predicted by our heuristic argument. There are two other regions associated with mismatched signs of the estimators, which do not lead to a simultaneous increase in separability and diversity. One region appears at $w_0 < 0$ and small ω : the negative-guidance window is too large, and even the mean collapses. The other one is relative to $w_0 > 0$ and high values of ω : guidance is always positive and, as predicted, variances must shrink.

Numerical validation of this theoretical picture is hindered by the fact that the exponential number of centroids does not allow us to simulate β large enough to avoid the guided-to-conditional transition. Nevertheless, Section D.2 provides a numerical validation of the same study on a joint Gaussian target, which presents a very similar phase diagram.

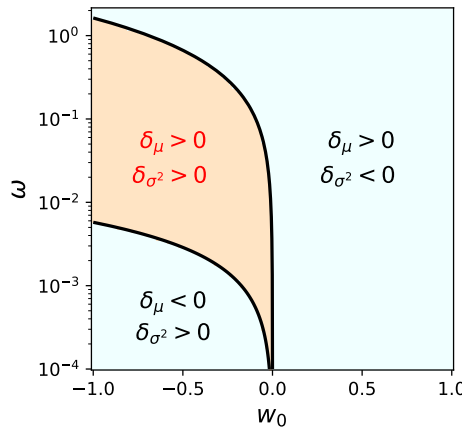


Figure 7. Phase diagram representing the effect of linear early-high CFG schedules with a negative guidance window, as function of w_0 and ω . The target variance is $\sigma^2 = 0.75$ and β has been set large enough to impede the transition to the conditional phase in the domain of interest. In the orange region means and variances are enlarged by guidance, implying gain in diversity and separability. The other regions either show loss of separability or tendency to shrink the mode variance.

6. Conclusions

We studied classifier-free guidance (CFG) through the lens of generative distortion, defined as the deviation between the CFG sampling distribution and the true conditional distribution. Combining experiments on real diffusion models with exact and approximate analyses of the dynamics, we showed that in high dimensions vanilla CFG generically expands conditional means while contracting variances, leading to systematic loss of diversity. For Gaussian distributions, we showed that distortion is always present, as long as the definition of classes is continuous. For mixtures of Gaussians, we identified a sharp regime distinction: distortion persists when the number of modes is exponential in dimension, but vanishes for sub-exponential mode counts, generalizing previous results (Pavasovich et al., 2025) and ruling out asymptotic alignment of CFG with conditional diffusion in multi-modal settings. These results suggest that distortion arises whenever classes are not sufficiently separated. Finally, we showed that standard CFG schedules with positive guidance cannot prevent variance shrinkage, and we proposed, based on our theory, a simple schedule incorporating a negative-guidance window that can simultaneously preserve class separability and enhance diversity. This prescription remains to be validated on learned score functions. Addressing more generic target distributions and providing an asymptotically exact mean field theory for the CFG dynamics are possible future directions for this line of research.

Impact Statement

The goal of this paper is to advance the theoretical understanding of generative modelling, with the future perspective of improving quality and controllability in real-world scenarios. In this respect, standard consideration on the societal impact of AI systems, and generative models in particular, with increased capabilities apply.

References

Achilli, B., Ventura, E., Silvestri, G., Pham, B., Raya, G., Krotov, D., Lucibello, C., and Ambrogioni, L. Losing dimensions: Geometric memorization in generative diffusion. *arXiv:2410.08727*, 2024.

Achilli, B., Ambrogioni, L., Lucibello, C., Mézard, M., and Ventura, E. Memorization and generalization in generative diffusion under the manifold hypothesis. *Journal of Statistical Mechanics: Theory and Experiment*, 2025(7):073401, 2025.

Anderson, B. D. Reverse-time diffusion equation models. *Stochastic Processes and their Applications*, 12(3):313–326, 1982.

Ban, Y., Wang, R., Zhou, T., Cheng, M., Gong, B., and Hsieh, C. Understanding the impact of negative prompts: When and how do they take effect? *Computer Vision – ECCV 2024: 18th European Conference*, 2024.

Biroli, G. and Mézard, M. Generative diffusion in very large dimensions. *Journal of Statistical Mechanics: Theory and Experiment*, 2023(9):093402, 2023.

Biroli, G., Bonnaire, T., de Bortoli, V., and Mézard, M. Dynamical regimes of diffusion models. *Nature Communications*, 15(1):9957, 2024.

Blattmann, A., Rombach, R., Ling, H., Dockhorn, T., Wook Kim, S., Fidler, S., and Kreis, K. Align your latents: High-resolution video synthesis with latent diffusion models. In *Conference on Computer Vision and Pattern Recognition*, 2023.

Bradley, A. and Nakkiran, P. Classifier-free guidance is a predictor-corrector. *International Conference on Learning Representations*, 2025.

Chen, S., Chewi, S., Li, J., Li, Y., Salim, A., and Zhang, A. Sampling is as easy as learning the score: theory for diffusion models with minimal data assumptions. *International Conference on Learning Representations*, 2022.

Chidambaram, M., Gatmiry, K., Chen, S., Lee, H., and Lu, J. What does guidance do? a fine-grained analysis in a simple setting. *Advances in Neural Information Processing Systems*, 2024.

Chung, H., Kim, J., Park, G. Y., Nam, H., and Ye, J. Cfg++: Manifold-constrained classifier free guidance for diffusion models. *International Conference on Learning Representations*, 2025.

Derrida, B. Random-energy model: An exactly solvable model of disordered systems. *Physical Review B*, 24(5): 2613–2626, 1981.

Dhariwal, P. and Nichol, A. Diffusion models beat gans on image synthesis. *Advances in Neural Information Processing Systems*, 2021.

Fu, H., Yang, Z., Wang, M., and Chen, M. Unveil conditional diffusion models with classifier-free guidance: A sharp statistical theory. *arXiv:2403.11968*, 2024.

George, A. J., Veiga, R., and Macris, N. Analysis of diffusion models for manifold data. *arXiv:2502.04339*, 2025.

Ho, J. and Salimans, T. Classifier-Free Diffusion Guidance. *Advances in Neural Information Processing Systems*, 2022.

Ho, J., Jain, A., and Abbeel, P. Denoising diffusion probabilistic models. In *Neural Information Processing Systems*. NeurIPS, 2020.

Ho, J., Salimans, T., Gritsenko, A., Chan, W., Norouzi, M., and Fleet, D. J. Video diffusion models. *arXiv preprint arXiv:2204.03458*, 2022.

Hyvärinen, A. and Dayan, P. Estimation of non-normalized statistical models by score matching. *Journal of Machine Learning Research*, 6(4), 2005.

Jiao, Y., Chen, Y., and Li, G. Towards a unified framework for guided diffusion models. *arXiv:2512.04985*, 2025.

Jin, C., Shi, Q., and Gu, Y. Stage-wise dynamics of classifier-free guidance in diffusion models. *arXiv:2509.22007*, 2025a.

Jin, C., Xiao, Z., Liu, C., and Gu, Y. Angle domain guidance: Latent diffusion requires rotation rather than extrapolation. *International Conference on Learning Representations*, 2025b.

Koulischer, F., Deleu, J., Raya, G., Demeester, T., and Ambrogioni, L. Dynamic negative guidance of diffusion models. *International Conference on Learning Representations*, 2025.

Li, G. and Jiao, Y. Provable efficiency of guidance in diffusion models for general data distribution. *International Conference on Learning Representations*, 2025.

Li, X., Wang, R., and Qu, Q. Towards understanding the mechanisms of classifier-free guidance. *Advances in Neural Information Processing Systems*, 2025.

Lucibello, C. and Mézard, M. The Exponential Capacity of Dense Associative Memories. *Physical Review Letters*, 132:077301, 2024.

Pavasovich, K. L., Verbeek, J., Biroli, G., and Mézard, M. Understanding classifier-free guidance:high-dimensional theory and non-linear generalizations. *arXiv:2502.07849*, 2025.

Raya, G. and Ambrogioni, L. Spontaneous symmetry breaking in generative diffusion models. In *Neural Information Processing Systems*. Advances in Neural Information Processing Systems, 2023.

Rombach, R., Blattmann, A., Lorenz, D., Esser, P., and Ommer, B. High-resolution image synthesis with latent diffusion models. *IEEE/CVF Conference on Computer Vision and Pattern Recognition*, 2022.

Sadat, S., Hilliges, O., and Weber, R. M. Eliminating over-saturation and artifacts of high guidance scales in diffusion models. *International Conference on Learning Representations*, 2025.

Saharia, C., Chan, W., Saxena, S., Li, L., Whang, J., Denton, E., Ghasemipour, K., Ayan, B. K., Mahdavi, S., Goncalves Lopes, R., Salimans, T., Ho, J., Fleet, D. J., and Norouzi, M. Photorealistic text-to-image diffusion models with deep language understanding. *Advances in Neural Information Processing Systems*, 2022.

Shen, D., Song, G., Xue, Z., Wang, F., and Liu, Y. Rethinking the spatial inconsistency in classifier-free diffusion guidance. *IEEE Conference on Computer Vision and Pattern Recognition*, 2024.

Singer, U., Polyak, A., Hayes, T., Yin, X., An, J., Zhang, S., Hu, Q., Yang, H., Ashual, O., Gafni, O., Parikh, D., Gupta, S., and Taigman, Y. Make-a-video: Text-to-video generation without text-video data. *arXiv:2209.14792*, 2022.

Sohl-Dickstein, J., Weiss, E. A., Maheswaranathan, N., and Ganguli, S. Deep unsupervised learning using nonequilibrium thermodynamics. In *International Conference on Machine Learning*. ICML, 2015.

Song, Y. and Ermon, S. Generative modeling by estimating gradients of the data distribution. *Advances in Neural Information Processing Systems*, 2019.

Song, Y., Sohl-Dickstein, J., Kingma, D. P., Kumar, A., Ermon, S., and Poole, B. Score-Based Generative Modeling through Stochastic Differential Equations. 2021.

Ventura, E., Achilli, B., Silvestri, G., Lucibello, C., and Ambrogioni, L. Manifolds, random matrices and spectral gaps: The geometric phases of generative diffusion. *International Conference on Learning Representations*, 2025.

Vincent, P. A Connection Between Score Matching and Denoising Autoencoders. *Neural Computation*, 23(7): 1661–1674, 2011.

Wang, X., Dufour, N., Andreou, N., Cani, M.-P., Abrevaya, V. F., Picard, D., and Kalogeiton, V. Analysis of classifier-free guidance weight schedulers. *Transactions on Machine Learning Research*, 2024.

Wu, Y., Chen, M., Li, Z., Wang, M., and Wei, Y. Theoretical insights for diffusion guidance: A case study for gaussian mixture models. *International Conference on Machine Learning*, 2024.

Yang, S. et al. Score-based generative modeling through stochastic differential equations. In *International Conference on Learning Representations*, 2021.

A. Multivariate Gaussian Data

Consider the data distribution

$$p_0(\mathbf{c}, \mathbf{x}) = \mathcal{N}\left(\begin{pmatrix} \mathbf{c} \\ \mathbf{x} \end{pmatrix}; \mathbf{0}, \Sigma\right), \quad \Sigma = \begin{pmatrix} \Sigma_{cc} & \Sigma_{cx} \\ \Sigma_{xc} & \Sigma_{xx} \end{pmatrix}, \quad (36)$$

defined on a d dimensional ambient space, where $\mathbf{c} \in \mathbb{R}^{d_1}$ and $\mathbf{x} \in \mathbb{R}^{d_2}$ with $d_2 + d_1 = d$ and $\Sigma_{xc} = \Sigma_{cx}^\top$. We consider a variance-exploding forward process (Achilli et al., 2024; Ventura et al., 2025), namely

$$\begin{pmatrix} \mathbf{c}_0 \\ \mathbf{x}_0 \end{pmatrix} \sim p_0, \quad \begin{pmatrix} \mathbf{c}_t \\ \mathbf{x}_t \end{pmatrix} = \begin{pmatrix} \mathbf{c}_0 \\ \mathbf{x}_0 \end{pmatrix} + \sqrt{t} \boldsymbol{\epsilon}_t, \quad \boldsymbol{\epsilon}_t \sim \mathcal{N}(0, I_d). \quad (37)$$

We call $p_t(\mathbf{c}_t, \mathbf{x}_t)$ the joint distribution of variables $(\mathbf{c}_t, \mathbf{x}_t)$, that is

$$p_t(\mathbf{c}_t, \mathbf{x}_t) = \int d\mathbf{c}_0 d\mathbf{x}_0 p_0(\mathbf{c}_0, \mathbf{x}_0) p(\mathbf{c}_t, \mathbf{x}_t | \mathbf{c}_0, \mathbf{x}_0) = \int d\mathbf{c}_0 d\mathbf{x}_0 \mathcal{N}(\mathbf{c}_0, \mathbf{x}_0; \mathbf{0}, \Sigma) \mathcal{N}(\mathbf{c}_t, \mathbf{x}_t; \mathbf{x}_0, tI_d) = \mathcal{N}(\mathbf{c}_t, \mathbf{x}_t; \mathbf{0}, \Sigma + tI_d) \quad (38)$$

We now pin a vector of features \mathbf{c} in the d_1 -dimensional subset of the ambient space, and we call it *class*. The sampling distribution conditioned with respect to such class reads

$$p_t(\mathbf{x}_t | \mathbf{c}) = \int p_0(\mathbf{x}_0 | \mathbf{c}) p(\mathbf{x}_t | \mathbf{x}_0) d\mathbf{x}_0 \quad (39)$$

$$= \int \mathcal{N}(\mathbf{x}_0; \Sigma_{xc} \Sigma_{cc}^{-1} \mathbf{c}, \Sigma_{x|c}) \mathcal{N}(\mathbf{x}_t; \mathbf{x}_0, tI_{d_2}) d\mathbf{x}_0 \quad (40)$$

$$= \mathcal{N}(\mathbf{x}_t; \Sigma_{xc} \Sigma_{cc}^{-1} \mathbf{c}, \Sigma_{x|c} + tI_{d_2}) = \mathcal{N}(\mathbf{x}_t; \Sigma_{cx}^\top \Sigma_{cc}^{-1} \mathbf{c}, \Sigma_{x|c}^t), \quad (41)$$

with

$$\Sigma_{x|c}^t = \Sigma_{xx} - \Sigma_{cx}^\top \Sigma_{cc}^{-1} \Sigma_{cx} + tI_{d_2}. \quad (42)$$

Therefore we can rewrite the full conditional density of \mathbf{x}_t as

$$p_t(\mathbf{c}_t, \mathbf{x}_t | \mathbf{c}) = \frac{1}{Z_t} \exp -\frac{1}{2} (\mathbf{x}_t - \boldsymbol{\mu})^\top (\tilde{\Sigma}_t)^{-1} (\mathbf{x}_t - \boldsymbol{\mu}), \quad (43)$$

where the observables become

$$Z_t = (2\pi)^{d/2} \det(\tilde{\Sigma}_t)^{1/2}, \quad (44)$$

$$\boldsymbol{\mu} = (\mathbf{c}, \Sigma_{cx}^\top \Sigma_{cc}^{-1} \mathbf{c}), \quad (45)$$

$$\tilde{\Sigma}_t = \begin{pmatrix} tI_{d_1} & 0 \\ 0 & \Sigma_{x|c}^t \end{pmatrix}. \quad (46)$$

Let us restrict to the d_2 -dimensional sub-space relative to \mathbf{x} . One has

$$p(\mathbf{x}_t | \mathbf{c}) = \mathcal{N}(\mathbf{x}_t; \boldsymbol{\mu}, \Sigma_{x|c}^t), \quad (47)$$

$$p(\mathbf{x}_t) = \mathcal{N}(\mathbf{x}_t; \mathbf{0}, \Sigma_{xx}^t) \quad (48)$$

where

$$\boldsymbol{\mu} = \Sigma_{cx}^\top \Sigma_{cc}^{-1} \mathbf{c} \quad (49)$$

$$\Sigma_{xx}^t = \Sigma_{xx} + tI_{d_2} \quad (50)$$

$$\Sigma_{x|c}^t = \Sigma_{x|c} + tI_{d_2} \quad (51)$$

$$\Sigma_{x|c} = \Sigma_{xx} - \Sigma_{cx}^\top \Sigma_{cc}^{-1} \Sigma_{cx} \quad (52)$$

The relative score function then become

$$\nabla_{\mathbf{x}} \log p(\mathbf{x}_t | \mathbf{c}) = - \left(\Sigma_{x|c}^t \right)^{-1} (\mathbf{x}_t - \boldsymbol{\mu}), \quad (53)$$

$$\nabla_{\mathbf{x}} \log p(\mathbf{x}_t) = - \left(\Sigma_{xx}^t \right)^{-1} \mathbf{x}_t. \quad (54)$$

As a consequence, the guided score becomes

$$\tilde{s}_t(\mathbf{x}_t | \mathbf{c}) = (1 + w) \nabla_{\mathbf{x}} \log p_t(\mathbf{x}_t | \mathbf{c}) - w \nabla_{\mathbf{x}} \log p_t(\mathbf{x}_t). \quad (55)$$

We want to find the probability distribution $\tilde{p}_t(\mathbf{x}_t | \mathbf{c})$ that samples the configurations generated by the following reverse-time SDE

$$d\mathbf{x}_t = -\tilde{s}_t(\mathbf{x}_t | \mathbf{c}) dt + dW_t. \quad (56)$$

Equation (56) can be rewritten explicitly as

$$d\mathbf{x}_t = -A(t)\mathbf{x}_t dt - B(t)\boldsymbol{\mu} dt + dW_t, \quad (57)$$

where

$$A(t) = -(1 + w) \left(\Sigma_{x|c}^t \right)^{-1} + w \left(\Sigma_{xx}^t \right)^{-1}, \quad (58)$$

$$B(t) = (1 + w) \left(\Sigma_{x|c}^t \right)^{-1}. \quad (59)$$

Integrating Eq. (9) backward in time brings to

$$\mathbf{x}_t = M(t, T)\mathbf{x}_T + \int_t^T M(t, t') B(t') \boldsymbol{\mu} dt' + \int_t^T M(t, t') dW_{t'}. \quad (60)$$

where we defined the matrix kernel

$$M(t_1, t_2) = e^{\int_{t_1}^{t_2} A(t') dt'}. \quad (61)$$

Let us now evaluate

$$\int_{t_1}^{t_2} A(t) dt = \int_{t_1}^{t_2} \left[-(1 + w)(\Sigma_{x|c}^t)^{-1} + w(\Sigma_{xx}^t)^{-1} \right] dt = \int_{t_1}^{t_2} \left[-\frac{1 + w}{\Sigma_{x|c} + tI_{d_2}} + \frac{w}{\Sigma_{xx} + tI_{d_2}} \right] dt \quad (62)$$

$$= \log \left[(\Sigma_{x|c} + t_2 I_{d_2})^{-(1+w)} (\Sigma_{x|c} + t_1 I_{d_2})^{1+w} \right] + \log \left[(\Sigma_{xx} + t_2 I_{d_2})^w (\Sigma_{xx} + t_1 I_{d_2})^{-w} \right] \quad (63)$$

Let us assume for simplicity that Σ_{xx} and $\Sigma_{x|c}$ commute. We get

$$M(t_1, t_2) = Z(t_1) Z(t_2)^{-1} \quad (64)$$

$$Z(t) = (\Sigma_{x|c} + tI_{d_2})^{1+w} (\Sigma_{xx} + tI_{d_2})^{-w} \quad (65)$$

We are interested in the asymptotic limit $T \rightarrow \infty$, with appropriate initial condition $\mathbf{x}_T \sim \mathcal{N}(\boldsymbol{\mu}, T I_{d_2})$. Since Eq. (60) gives us the law $\tilde{p}_w(\mathbf{x}_t | \mathbf{x}_T)$, we should convolve with \mathbf{x}_T to obtain the marginal for \mathbf{x}_t . We can argue though (and check for the $w = 0$ case) that for large T the initial condition becomes irrelevant, that is $\tilde{p}_t(\mathbf{x}_t | \mathbf{x}_T) \approx \tilde{p}_t(\mathbf{x}_t)$. In practice, we can focus on solving

$$\mathbf{x}_t = \int_t^{+\infty} M(t, t') B(t') \boldsymbol{\mu} dt' + \int_t^{+\infty} M(t, t') d\mathbf{W}_{t'}. \quad (66)$$

We see that \mathbf{x}_t is Gaussian, with mean and covariance given by

$$\boldsymbol{\mu}_w(t) = \int_t^{+\infty} M(t, t') B(t') \boldsymbol{\mu} dt' = Z(t) \int_t^{+\infty} Z^{-1}(t') B(t') \boldsymbol{\mu} dt' \quad (67)$$

$$\Sigma_w(t) = \int_t^{+\infty} M^2(t, t') dt' = Z^2(t) \int_t^{+\infty} Z^{-2}(t') dt' \quad (68)$$

A.1. Computation of $\boldsymbol{\mu}_w$

Consider $\boldsymbol{\mu}_w$ defined in Eq. (67). Call $R = \Sigma_{xx}$ and $S = \Sigma_{x|c}$ and assume they commute. Then

$$\int_{t_1}^{t_2} Z^{-1}(t') B(t') dt' = (1+w) \int_{t_1}^{t_2} (R + tI_{d_2})^w (S + tI_{d_2})^{-2-w} dt = P \text{ diag}(e_1(t_1, t_2), \dots, e_{d_2}(t_1, t_2)) P^{-1}, \quad (69)$$

where P is the unitary matrix collecting the common eigenvectors to R and S and

$$e_i(t_1, t_2) = \begin{cases} \frac{1}{(s_i - r_i)} \left[\left(\frac{r_i + t_2}{s_i + t_2} \right)^{w+1} - \left(\frac{r_i + t_1}{s_i + t_1} \right)^{w+1} \right], & s_i \neq r_i, \\ (1+w) \left[\frac{1}{r_i + t_1} - \frac{1}{r_i + t_2} \right], & s_i = r_i. \end{cases} \quad (70)$$

This is the sought-after closed-form solution, valid as long as $(s_i + t) \neq 0$ on $[t_1, t_2]$. By substituting $t_1 = t$ and $t_2 = T$ and plugging the last calculation into Eq. (67) we obtain

$$\boldsymbol{\mu}_w(t, T) = \sum_{i=1}^{d_2} \lambda_i(t, T) (\mathbf{v}^{(i),\top} \boldsymbol{\mu}) \mathbf{v}^{(i)}, \quad (71)$$

where $\{\mathbf{v}^{(i)}\}_{i=1}^{d_2}$ is the basis of eigenvectors shared between Σ_{xx} and $\Sigma_{x|c}$ and

$$\lambda_i(t, T) = \begin{cases} \frac{1}{(s_i - r_i)} \left[\left(\frac{r_i + T}{s_i + T} \right)^{w+1} \frac{(s_i + t)^{w+1}}{(r_i + t)^w} - r_i - t \right], & s_i \neq r_i, \\ (1+w) \left[1 - \frac{r_i + t}{r_i + T} \right], & s_i = r_i. \end{cases} \quad (72)$$

In the limit $T \rightarrow \infty$ the same variables become

$$\boldsymbol{\mu}_w(t) = \sum_{i=1}^{d_2} \lambda_i(t) (\mathbf{v}^{(i),\top} \boldsymbol{\mu}) \mathbf{v}^{(i)}, \quad (73)$$

$$\lambda_i(t) = \begin{cases} \frac{1}{(s_i - r_i)} \left[\frac{(s_i + t)^{w+1}}{(r_i + t)^w} - (r_i + t) \right], & s_i \neq r_i, \\ 1 + w & s_i = r_i. \end{cases} \quad (74)$$

Since $s_i/r_i < 1 \forall i$ it can be deduced that $\lambda_i(t) > 1 \forall i, t$. By rewriting the conditional mean as

$$\boldsymbol{\mu} = \sum_{i=1}^{d_2} (\mathbf{v}^{(i),\top}, \boldsymbol{\mu}) \mathbf{v}^{(i)}, \quad (75)$$

and comparing it with the expression of $\boldsymbol{\mu}_w$ in Eq. (71) we notice that $\|\boldsymbol{\mu}_w\| > \|\boldsymbol{\mu}\| \forall w$, that means that means are always expanded by the CFG in this framework at $t = 0$.

A.2. Computation of Σ_w

Consider Σ_w defined in Eq. (68). Call $R = \Sigma_{xx}$ and $S = \Sigma_{x|c}$ and assume they commute. For each eigenvalue pair (r_i, s_i) of (R, S) , the integral is diagonal in the basis that diagonalizes R and S . Hence

$$\int_{t_1}^{t_2} Z^{-2}(t') dt' = \int_{t_1}^{t_2} (R + tI_{d_2})^{2w} (S + tI_{d_2})^{-2-2w} dt = P \operatorname{diag}(e_1(t_1, t_2), \dots, e_{d_2}(t_1, t_2)) P^{-1}, \quad (76)$$

where P is the unitary matrix collecting the common eigenvectors to R and S and

$$e_i(t_1, t_2) = \begin{cases} \frac{1}{(2w+1)(s_i - r_i)} \left[\left(\frac{r_i + t_2}{s_i + t_2} \right)^{2w+1} - \left(\frac{r_i + t_1}{s_i + t_1} \right)^{2w+1} \right], & \text{if } s_i \neq r_i, \\ \frac{1}{s_i + t_1} - \frac{1}{s_i + t_2}, & \text{if } s_i = r_i. \end{cases} \quad (77)$$

That is valid as long as $(s_i + t) \neq 0$ over $[t_1, t_2]$. By substituting $t_1 = t$ and $t_2 = T$ and plugging the last calculation into Eq. (68) we obtain

$$\Sigma_w(t, T) = \sum_{i=1}^{d_2} \Lambda_i(t, T) (s_i + t) \mathbf{v}^{(i)} \mathbf{v}^{(i), \top}, \quad (78)$$

where $\{\mathbf{v}^{(i)}\}_{i=1}^{d_2}$ is the basis of eigenvectors shared between Σ_{xx} and $\Sigma_{x|c}$ and

$$\Lambda_i(t, T) = \begin{cases} \frac{1}{(2w+1)(s_i - r_i)} \left[\left(\frac{r_i + T}{s_i + T} \right)^{2w+1} \frac{(s_i + t)^{1+2w}}{(r_i + t)^{2w}} - (r_i + t) \right], & \text{if } s_i \neq r_i, \\ 1 - \frac{s_i + t}{s_i + T}, & \text{if } s_i = r_i. \end{cases} \quad (79)$$

In the limit $T \rightarrow \infty$ the same variables become

$$\Sigma_w(t) = \sum_{i=1}^{d_2} \Lambda_i(t) (s_i + t) \mathbf{v}^{(i)} \mathbf{v}^{(i), \top}, \quad (80)$$

and

$$\Lambda_i(t) = \begin{cases} \frac{1}{(2w+1)(s_i - r_i)} \left[\frac{(s_i + t)^{1+2w}}{(r_i + t)^{2w}} - (r_i + t) \right], & \text{if } s_i \neq r_i, \\ 1 & \text{if } s_i = r_i. \end{cases} \quad (81)$$

One can notice that this quantity is smaller than unity for any choice of $w > 0$ and $s_i/r_i < 1$. By writing the conditional covariance according to its spectral decomposition

$$\Sigma_{x|c} = \sum_{i=1}^{d_2} s_i \mathbf{v}^{(i)} \mathbf{v}^{(i), \top}, \quad (82)$$

and comparing it with the expression of the guided covariance Σ_w in Eq. (80) we realize that covariances always undergo contraction under CFG in this setup at $t = 0$.

B. Data from a Mixture of Gaussians

Consider the Mixture of Gaussians

$$p_0(\mathbf{x}) = \frac{1}{M} \sum_{\mu=1}^M \mathcal{N}(\mathbf{x}; \mathbf{c}^\mu, \sigma^2) \quad (83)$$

as the target distribution of our diffusion model. The conditional distribution with respect to one class \mathbf{c}^1 is going to be one Gaussian from the mixture, namely

$$p_0(\mathbf{x}|\mathbf{c}^1) = \mathcal{N}(\mathbf{x}; \mathbf{c}^1, \sigma^2). \quad (84)$$

The time evolution of the target distribution according to a variance-exploding forward process will read

$$p_t(\mathbf{x}_t) = \frac{1}{M} \sum_{\mu=1}^M \mathcal{N}(\mathbf{x}_t; \mathbf{c}^\mu, \sigma^2 + t), \quad (85)$$

$$p_t(\mathbf{x}_t | \mathbf{c}^1) = \mathcal{N}(\mathbf{x}_t; \mathbf{c}^1, \sigma^2 + t). \quad (86)$$

The guided backward process is described by the following SDE

$$d\mathbf{x}_t = -\tilde{s}_t(\mathbf{x}_t | \mathbf{c}^1) dt + dW_t, \quad (87)$$

where the guided score function is given by

$$\tilde{s}_t(\mathbf{x}) = (1+w)s_t(\mathbf{x} | \mathbf{c}^1) - w s_t(\mathbf{x}), \quad (88)$$

where dW_t is Brownian noise, and w being our guidance level. The same SDE can be rewritten in terms of an effective diffusion potential as

$$d\mathbf{x}_t = \nabla_{\mathbf{x}} V_{\text{eff}}(\mathbf{x}_t) dt + dW_t, \quad (89)$$

where

$$V_{\text{eff}}(\mathbf{x}_t) = -\log \left[\frac{p_t(\mathbf{x}_t | \mathbf{c}^1)^{1+w}}{p_t(\mathbf{x}_t)^w} \right] = \log \left[e^{\frac{(1+w)}{2(\sigma^2+t)} \|\mathbf{x}_t - \mathbf{c}^1\|^2} \left(\frac{1}{M} \sum_{\mu=1}^M e^{-\frac{1}{2(\sigma^2+t)} \|\mathbf{x}_t - \mathbf{c}^\mu\|^2} \right)^w \right] + \frac{d}{2} \log(2\pi t), \quad (90)$$

Let us define the name of modes in the mixture of Gaussians as $M = e^{\beta(d) \cdot d}$, where $\beta(d)$ can arbitrarily scale with the dimension d . The same potential can be expressed in terms of a conditional and a guided part as

$$V_{\text{eff}}(\mathbf{x}_t) = V_{\text{cond}}(\mathbf{x}_t) + V_{\text{guided}}(\mathbf{x}_t) \quad (91)$$

$$= \frac{1}{2} \frac{\|\mathbf{x}_t - \mathbf{c}^1\|^2}{\sigma^2 + t} + \frac{d}{2} \log(2\pi t) - w \left[d\beta(d) - \log \left(1 + \sum_{\mu>1}^M e^{-\frac{1}{2(\sigma^2+t)} (\|\mathbf{x}_t - \mathbf{c}^\mu\|^2 - \|\mathbf{x}_t - \mathbf{c}^1\|^2)} \right) \right]. \quad (92)$$

B.1. The Random Energy Model (REM) formalism

Let us introduce the tools needed to solve a generic REM, following (Lucibello & Mézard, 2024; Derrida, 1981).

Let us consider $M = e^{\beta d}$ (or equivalently $M = e^{\beta d} - 1$) i.i.d. energy levels $\epsilon^\mu \sim p(\epsilon | \omega)$, where we extend the typical REM setting allowing for a common source of quenched disorder $\omega \sim p_\omega$. The goal is to compute the average asymptotic free energy of the system, defined by

$$\phi_\beta(\lambda) = \lim_{d \rightarrow \infty} \frac{1}{\lambda d} \mathbb{E} \log \sum_\mu e^{\lambda d \epsilon^\mu} \quad (93)$$

We shall assume that the probability distribution of the energy levels is such that, with probability one over the choice of ω when $d \rightarrow \infty$ the cumulant generating function has a well defined limit: $\lim_{d \rightarrow \infty} \frac{1}{N} \log \mathbb{E}_{\epsilon | \omega} e^{\lambda d \epsilon}$ exists, and the distribution over the choices of ω concentrates around its mean. Then we define the typical cumulant generating function and its Legendre transform::

$$\zeta(\lambda) = \lim_{d \rightarrow \infty} \frac{1}{d} \mathbb{E}_\omega \log \mathbb{E}_{\epsilon | \omega} e^{\lambda d \epsilon}, \quad (94)$$

$$s(\epsilon) = \sup_\lambda \epsilon \lambda - \zeta(\lambda). \quad (95)$$

The total entropy of the system is $\Sigma(\epsilon) = \alpha - s(\epsilon)$. Depending on the value of $\Sigma(\epsilon)$, the REM displays a separation into two thermodynamic phases: an *uncondensed* phase where the system can populate an exponential number of energy levels, at lower values of λ ; a *condensed* phase where the system is able to populate a unique energy state, at higher values of λ .

Let us define the quantities $\epsilon_*(\alpha)$ and $\lambda_*(\beta)$ respectively as the maximum value of the energy levels in the uncondensed phase, obtained as the largest root of $\Sigma(\epsilon_*) = 0$, and the condensation threshold. Notice that we are seeking for the maximum energy,

by definition of the free-energy function in Eq. (93). In the uncondensed phase, i.e. when $\lambda < \lambda_*(\beta)$, the dominating energy level $\tilde{\epsilon}(\lambda)$ is obtained as the stationary point of $\lambda\epsilon - s(\epsilon)$, and by the Legendre transform definition of $\zeta(\lambda)$ this is equivalent to $\tilde{\epsilon}(\lambda) = \zeta'(\lambda)$. The entropy of the dominating state can be rewritten as $\Sigma(\tilde{\epsilon}(\lambda)) = \beta - s(\tilde{\epsilon}(\lambda)) = \beta + \zeta(\lambda) - \lambda\zeta'(\lambda)$, so the condensation threshold $\lambda_*(\alpha)$ is obtained from the condensation condition

$$\beta + \zeta(\lambda_*) - \lambda_*\zeta'(\lambda_*) = 0. \quad (96)$$

Finally, the free energy is given by

$$\phi_\beta(\lambda) = \begin{cases} \frac{\beta + \zeta(\lambda)}{\lambda} & \lambda < \lambda_*(\beta), \\ \epsilon_*(\alpha) & \lambda \geq \lambda_*(\beta). \end{cases} \quad (97)$$

B.2. REM analysis of the Guided Potential

The guided contribution can be re-expressed in terms of the free-energy of a Random Energy Model (REM) (Derrida, 1981). The guided potential now reads

$$V_{\text{guided}}(\mathbf{x}_t) \approx -w \left[d\beta(d) - \log \left(1 + e^{d\phi_t(\mathbf{x}_t|\mathbf{c}^1)} \right) \right]. \quad (98)$$

where the REM free-energy is given by

$$\phi_t(\mathbf{x}_t|\mathbf{c}^1) = \begin{cases} \beta(d) + \zeta_{t,1}(\mathbf{x}_t|\mathbf{c}^1) & 1 < \lambda_*(\beta, d, \sigma^2, t), \\ \zeta'_{t,\lambda_*}(\mathbf{x}_t|\mathbf{c}^1) & 1 \geq \lambda_*(\beta, d, \sigma^2, t). \end{cases} \quad (99)$$

The moment-generating function reads

$$\zeta_{t,\lambda}(\mathbf{x}_t|\mathbf{c}^1) = \lim_{d \rightarrow \infty} \frac{1}{d} \log \left(\mathbb{E}_{\mathbf{c}} e^{-\frac{\lambda}{2(\sigma^2+t)}(\|\mathbf{x}_t - \mathbf{c}\|^2 - \|\mathbf{x}_t - \mathbf{c}^1\|^2)} \right) \quad (100)$$

$$= \frac{\lambda}{2(\sigma^2+t)} \lim_{d \rightarrow \infty} \frac{\|\mathbf{c}^1\|^2}{d} - \frac{\lambda}{\sigma^2+t} \lim_{d \rightarrow \infty} \frac{\mathbf{x}_t \cdot \mathbf{c}^1}{d} + \lim_{d \rightarrow \infty} \log \left(\int \frac{d\mathbf{c}}{(2\pi)^{d/2}} e^{-\frac{1}{2}(1+\frac{\lambda}{\sigma^2+t})\|\mathbf{c}\|^2 + \frac{\lambda}{\sigma^2+t}\mathbf{x}_t \cdot \mathbf{c}} \right) \quad (101)$$

$$= \frac{\lambda}{2(\sigma^2+t)} \lim_{d \rightarrow \infty} \frac{\|\mathbf{x}_t - \mathbf{c}^1\|^2}{d} - \frac{1}{2} \log \left(1 + \frac{\lambda}{\sigma^2+t} \right) - \frac{\lambda}{2(\sigma^2+t+\lambda)} \lim_{d \rightarrow \infty} \frac{\|\mathbf{x}_t\|^2}{d}, \quad (102)$$

while its derivative is

$$\zeta'_{t,\lambda}(\mathbf{x}_t|\mathbf{c}^1) = \frac{1}{2(\sigma^2+t)} \lim_{d \rightarrow \infty} \frac{\|\mathbf{x}_t - \mathbf{c}^1\|^2}{d} - \frac{1}{2(\sigma^2+t+\lambda)} - \frac{\sigma^2+t}{2(\sigma^2+t+\lambda)^2} \lim_{d \rightarrow \infty} \frac{\|\mathbf{x}_t\|^2}{d}. \quad (103)$$

The condition for finding the threshold variable $\lambda_*(d)$ reads

$$\beta(d) + \zeta_{t,\lambda_*} - \lambda_* \zeta'_{t,\lambda_*} = \beta(d) - \frac{1}{2} \ln \left(1 + \frac{\lambda_*}{\sigma^2+t} \right) + \frac{\lambda_*}{2(\sigma^2+t+\lambda_*)} \left(1 - \frac{\lambda_*}{\sigma^2+t+\lambda_*} \lim_{d \rightarrow \infty} \frac{\|\mathbf{x}\|^2}{d} \right) = 0. \quad (104)$$

According to the physics of REM, the model enters a *conditional* phase as soon as $\phi_t(\mathbf{x}|\mathbf{c}^1) \leq 0$. Otherwise, the model explores an *guided* phase if $\lambda_* > 1$ or a *condensed* one if $\lambda_* \leq 1$. The expression for the diffusion potential in terms of the REM moment-generating function reads

$$V_{\text{eff}}(\mathbf{x}_t) = \begin{cases} \frac{1}{2} \frac{\|\mathbf{x}_t - \mathbf{c}^1\|^2}{\sigma^2+t} + \frac{d}{2} \log(2\pi t) + dw \zeta_{t,1}(\mathbf{x}_t|\mathbf{c}^1) & \text{(guided phase)} \\ -\frac{1}{2} \frac{\|\mathbf{x} - \mathbf{c}^1\|^2}{\sigma^2+t} - \frac{N}{2} \log(2\pi t) + w\beta N & \text{(conditional phase)} \\ -\frac{1}{2} \frac{\|\mathbf{x} - \mathbf{c}^1\|^2}{\sigma^2+t} - \frac{N}{2} \log(2\pi t) + wN \left[\beta - \zeta'_{t,\lambda_*}(\mathbf{x}|\mathbf{c}^1) \right] & \text{(condensed phase),} \end{cases} \quad (105)$$

while full effective potential becomes

$$V_{\text{eff}}(\mathbf{x}_t) = \begin{cases} -\frac{(1+w)}{2} \frac{\|\mathbf{x} - \mathbf{c}^1\|^2}{\sigma^2+t} + \frac{w\|\mathbf{x}\|^2}{2(\sigma^2+t+1)} - \frac{wN}{2} \log \left(1 + \frac{1}{\sigma^2+t} \right) - \frac{N}{2} \log(2\pi t) & \text{(guided phase)} \\ -\frac{1}{2} \frac{\|\mathbf{x} - \mathbf{c}^1\|^2}{\sigma^2+t} - \frac{N}{2} \log(2\pi t) + w\beta N & \text{(conditional phase)} \\ -\frac{(1+w)}{2} \frac{\|\mathbf{x} - \mathbf{c}^1\|^2}{\sigma^2+t} - \frac{N}{2} \log(2\pi t) + w \left[\beta N + \frac{\sigma^2+t}{2(\sigma^2+t+\lambda_*)^2} \|\mathbf{x}\|^2 + \frac{1}{2(\sigma^2+t+\lambda_*)} \right] & \text{(condensed phase)} \end{cases} \quad (106)$$

The local minimum of the potential is unique at any time, and it is given by

$$\mathbf{x}^*(t) = \begin{cases} \frac{(1+w)(\sigma^2+t+1)}{w+\sigma^2+t+1} \mathbf{c}^1 & \text{(guided phase)} \\ \mathbf{c}^1 & \text{(conditional phase)} \\ \left[1 + \frac{w}{1+w} \left(\frac{\sigma^2+t}{\sigma^2+t+\lambda_*} \right)^2 \right]^{-1} \mathbf{c}^1 & \text{(condensed phase).} \end{cases} \quad (107)$$

In absence of correlated centroids, we expect the system to never enter the condensed phase of the potential, as a consequence of the isotropic nature of the stochastic process: the condensation and collapse transitions of the relative REM are going to coincide (see (Achilli et al., 2025) for a more rigorous justification based on the Nishimori conditions applied to the problem). Hence the transition between the guided phase and the conditional one occurs when the REM free-energy of the model changes sign. We name the transition time, in continuity with the literature, *speciation time* t_s (Biroli et al., 2024). Our transition condition thus reads

$$\lim_{d \rightarrow \infty} [\beta(d) + \zeta_{t_s}(\sigma^2, w)] = 0, \quad (108)$$

where ζ_t depends on the specific trajectory \mathbf{x}_t and also on the norm of \mathbf{c}^1 .

C. Mean Field description of CFG

We want to solve the system of d independent SDEs represented by

$$d\mathbf{x}_t = \mathbf{x}_t a(t) dt + b(t) dt + d\mathbf{w}_t, \quad (109)$$

where functions $a(t), b(t)$ change from phase to phase in the REM analysis. Such SDEs can be solved component by component using the integrating factor method. The procedure corresponds to first define an auxiliary function

$$\Phi(t) = \exp \left[- \int_0^s ds a(s) \right]. \quad (110)$$

By simplicity, let us consider one single component of the vectors and drop the index label. Each SDE now reads

$$x_t = \Phi^{-1}(t)\Phi(T) x_T + \Phi(t)^{-1} \int_T^t ds \Phi(s)b(s) + \Phi^{-1}(t) \int_T^t ds \Phi(s)\xi(s), \quad (111)$$

where we have rewritten the noise term as $dw_t = \xi(t)dt$ with $\langle \xi(t) \rangle_\xi = 0$ and $\langle \xi(t)\xi(t') \rangle_\xi = \delta(t-t')$. Let us derive, in Sections C.1, C.2, C.3 the solution \mathbf{x}_t , and its first two moments, separately in the three dynamic phases obtained from the REM analysis of the diffusion potential. Such moments are defined with respect to the measure $\langle \cdot \rangle_\xi$ as

$$\boldsymbol{\mu}(t) = \langle \mathbf{x}(t) \rangle_\xi \quad (112)$$

$$\sigma^2(t) = \langle \|\mathbf{x}(t)\|^2 \rangle_\xi - \|\boldsymbol{\mu}(t)\|^2. \quad (113)$$

Section C.4 will be devoted to put all the pieces together and show how the entire trajectory, across the three phases, is derived.

C.1. Conditional phase

In this phase SDEs read

$$dx = \frac{x}{\sigma^2 + t} dt - \frac{c^1}{\sigma^2 + t} dt + dW_t \quad (114)$$

The auxiliary functions read

$$a(t) = \frac{1}{\sigma^2 + t}, \quad b(t) = -\frac{c^1}{\sigma^2 + t}, \quad \Phi(t) = \frac{\sigma^2}{\sigma^2 + t}. \quad (115)$$

The evolution equation reads

$$x_t = \frac{\sigma^2 + t}{\sigma^2 + T} x_T + \frac{T - t}{\sigma^2 + T} c^1 + (\sigma^2 + t) \int_T^t ds \frac{\xi(s)}{\sigma^2 + s}, \quad (116)$$

where x_T is the initial condition for the integration. From the isotropy of the process, the solution x_t must be normally distributed with mean

$$\mu(t) = \frac{\sigma^2 + t}{\sigma^2 + T} \mu(T) + \frac{T - t}{\sigma^2 + T} c^1, \quad (117)$$

and variance

$$\sigma^2(t) = \left(\frac{\sigma^2 + t}{\sigma^2 + T} \right)^2 \sigma^2(T) + (T - t) \frac{\sigma^2 + t}{\sigma^2 + T}. \quad (118)$$

C.2. Guided Phase

In this phase SDEs read

$$dx = x \frac{\sigma^2 + t + 1 + w}{(\sigma^2 + t)(\sigma^2 + t + 1)} dt - c^1 \frac{(1 + w)}{(\sigma^2 + t)} dt + dW_t \quad (119)$$

The auxiliary functions for the overlap read as

$$a(t) = \frac{\sigma^2 + t + 1 + w}{(\sigma^2 + t)(\sigma^2 + t + 1)}, \quad b(t) = -c^1 \frac{(1 + w)}{(\sigma^2 + t)}, \quad \Phi(t) = \frac{\sigma^2}{\sigma^2 + t} \left[\frac{\sigma^2 + 1 + t}{\sigma^2 + 1} \frac{\sigma^2}{\sigma^2 + t} \right]^w. \quad (120)$$

The evolution equation for the overlap thus reads as follows

$$x_t = x_T \left(\frac{\sigma^2 + t}{\sigma^2 + T} \right) \left[\frac{\sigma^2 + t}{\sigma^2 + T} \frac{\sigma^2 + 1 + T}{\sigma^2 + 1 + t} \right]^w + c^1 \frac{(\sigma^2 + t)^{(1+w)}}{(\sigma^2 + t + 1)^w} \left[\left(1 + \frac{1}{\sigma^2 + t} \right)^{1+w} - \left(1 + \frac{1}{\sigma^2 + T} \right)^{1+w} \right] \quad (121)$$

$$+ \frac{(\sigma^2 + t)^{w+1}}{(\sigma^2 + 1 + t)^w} \int_T^t ds \xi(s) \frac{(\sigma^2 + 1 + s)^w}{(\sigma^2 + s)^{w+1}} \quad (122)$$

where x_T is the initial condition for the integration. From the isotropy of the process, the solution x_t must be normally distributed with mean

$$\mu(t) = \left(\frac{\sigma^2 + t}{\sigma^2 + T} \right) \left[\frac{\sigma^2 + t}{\sigma^2 + T} \frac{\sigma^2 + 1 + T}{\sigma^2 + 1 + t} \right]^w \mu(T) + \frac{(\sigma^2 + t)^{(1+w)}}{(\sigma^2 + t + 1)^w} \left[\left(1 + \frac{1}{\sigma^2 + t} \right)^{1+w} - \left(1 + \frac{1}{\sigma^2 + T} \right)^{1+w} \right] c^1, \quad (123)$$

and variance

$$\sigma^2(t) = \left(\frac{\sigma^2 + t}{\sigma^2 + T} \right)^2 \left[\frac{\sigma^2 + t}{\sigma^2 + T} \frac{\sigma^2 + 1 + T}{\sigma^2 + 1 + t} \right]^{2w} \sigma^2(T) + \frac{(\sigma^2 + t)^{2w+2}}{(\sigma^2 + t + 1)^{2w}} \int_T^t ds \frac{(\sigma^2 + 1 + s)^{2w}}{(\sigma^2 + s)^{2w+2}} \quad (124)$$

$$= \left(\frac{\sigma^2 + t}{\sigma^2 + T} \right)^2 \left[\frac{\sigma^2 + t}{\sigma^2 + T} \frac{\sigma^2 + 1 + T}{\sigma^2 + 1 + t} \right]^{2w} \sigma^2(T) \quad (125)$$

$$+ \frac{(\sigma^2 + t)^{2w+2}}{(\sigma^2 + t + 1)^{2w}} \frac{1}{2w+1} \left[\left(1 + \frac{1}{\sigma^2 + t} \right)^{2w+1} - \left(1 + \frac{1}{\sigma^2 + T} \right)^{2w+1} \right]. \quad (126)$$

C.3. Condensed Phase

In this phase, SDEs read

$$dx = x \left[\frac{1 + w}{\sigma^2 + t} - \frac{w(\sigma^2 + t)}{(\sigma^2 + t + \lambda_*(t))^2} \right] dt - c^1 \frac{(1 + w)}{(\sigma^2 + t)} dt + dW_t \quad (127)$$

The auxiliary functions for the overlap read as

$$a(t) = \frac{1+w}{\sigma^2+t} - \frac{w(\sigma^2+t)}{(\sigma^2+t+\lambda_*(t))^2}, \quad b(t) = -c^1 \frac{(1+w)}{(\sigma^2+t)}, \quad \Phi(t) = \exp \left[- \int_0^t ds a(s) \right]. \quad (128)$$

The integrating factor cannot be computed in closed form, since $\lambda_*(t)$ is derived, for each time value, through the implicit function in Eq. (104). As a consequence this ODE must be integrated numerically.

C.4. Assembling the whole Diffusive Trajectory and Measuring Distortion

In order to derive the full trajectory of the system in the ambient space, as well as the distortion as a function of time, one has to take into account the transition among different phases of the potential.

All trajectories will be initialized at the time horizon $T \rightarrow \infty$. We can infer that, in this limit, the system always starts from the guided phase. In fact, from Eq. (104), one has

$$\lim_{T \rightarrow \infty} \frac{1}{2} \ln \left(1 + \frac{\lambda_*}{\sigma^2 + T} \right) - \frac{\lambda_*}{2(\sigma^2 + T + \lambda_*)} \left(1 - \frac{\lambda_*}{\sigma^2 + T + \lambda_*} \lim_{d \rightarrow \infty} \frac{\|\mathbf{x}\|^2}{d} \right) = \beta. \quad (129)$$

By choosing the variance for $\mathbf{x}(T)$ to be $\mathcal{O}(T)$, then the same condition becomes

$$\lim_{T \rightarrow \infty} \frac{\lambda_*(\lambda_* - 1)}{2T} = \beta, \quad (130)$$

As a consequence, the system always starts diffusing from the guided phase.

At this point we need to compute the transition time from guided phase to the conditional one, by solving the implicit equation (108). The explicit expression of the moment-generating function in the guided phase reads

$$\zeta_t(\sigma^2, w) = \frac{1}{2} \left(\frac{(\sigma^2+t)^{2w+1}}{(\sigma^2+t+1)^{2w}} - \frac{(\sigma^2+t)^{2w+2}}{(\sigma^2+t+1)^{2w+1}} \right) \left[\frac{1}{2w+1} \left[\left(1 + \frac{1}{\sigma^2+t} \right)^{2w+1} - 1 \right] + \left[\left(1 + \frac{1}{\sigma^2+t} \right)^{1+w} - 1 \right] \right] \quad (131)$$

$$+ \frac{1}{2(\sigma^2+t)} - \frac{(\sigma^2+t)^w}{(\sigma^2+t+1)^w} \left[\left(1 + \frac{1}{\sigma^2+t} \right)^{1+w} - 1 \right] - \frac{1}{2} \log \left(1 + \frac{1}{\sigma^2+t} \right) \quad (132)$$

Generally speaking, the order of magnitude of such time with respect to the ambient dimension d will depend on the nature of $\beta(d)$. We can recover the scaling behavior of t_s Vs d from a simple dimensional reasoning. Let us notice that $\zeta_t(\sigma^2, w)$ decreases monotonically in time and $\zeta_t(w) = -\frac{1+w}{t} + \mathcal{O}(\frac{1}{t^2})$ at large times t . As a consequence, if $\lim_{d \rightarrow \infty} \beta(d) = 0$, then we must have

$$t_s(w, d) = \mathcal{O} \left(\frac{1+w}{\beta(d)} \right). \quad (133)$$

This expression implies that the speciation time diverges when the number of modes in the mixture is sub-exponential. If the speciation time diverges, the system never effectively visits the guided phase, and we can envisage no final distortion of the target distribution. On the other hand, when the number of possible classes is exponentially large in d , $t_s = \mathcal{O}(1)$ and distortion is ensured.

The assembly of the whole trajectory can be done by integrating the backward SDE in the following order:

1. The **guided** phase SDE for $t \in [\max(0, t_s(w, \beta, \sigma^2)), T]$ with initial conditions $\mu(T) = \mathbf{0}$, $\sigma^2(T) = T$ and $T \rightarrow \infty$.
2. The **conditional** phase SDE for $t \in [0, \max(0, t_s(w, \beta, \sigma^2))]$ with initial conditions $\mu(T) = \mu(t_s)$ and $\sigma^2(T) = \sigma^2(t_s)$.

The operator $\max(0, t_s)$ means that, when $t_s < 0$ from the analysis, the system displays no speciation, because the modes of the mixture of Gaussians mutually merged, due to σ^2 or β being too large.

Eventually, to quantify the distortion performed in time by CFG on the data target distribution we introduce the following two observables

$$\delta_\mu(t) = \lim_{d \rightarrow \infty} \frac{\mathbf{c}^1 \cdot (\boldsymbol{\mu}_w(t) - \mathbf{c}^1)}{d}, \quad (134)$$

and

$$\delta_{\sigma^2}(t) = \frac{\sigma^2(t) - (\sigma^2 + t)}{\sigma^2 + t}. \quad (135)$$

The observable in Eq. (134) quantifies the distortion of the mean, while observable in Eq. (135) focuses on the distortion of the variance, always with respect to the conditional target distribution. Given these considerations, the starting distortion observables measure

$$\delta_\mu(t) = \frac{(\sigma^2 + t)^{1+w}}{(\sigma^2 + t + 1)^w} \left[\left(1 + \frac{1}{\sigma^2 + t} \right)^{1+w} - 1 \right] - 1, \quad (136)$$

$$\delta_{\sigma^2}(t) = \frac{1}{\sigma^2 + t} \left[\frac{(\sigma^2 + t)^{2w+2}}{(\sigma^2 + t + 1)^{2w}} \frac{1}{2w+1} \left[\left(1 + \frac{1}{\sigma^2 + t} \right)^{2w+1} - 1 \right] - (\sigma^2 - t) \right]. \quad (137)$$

The system might then enter the conditional phase at a time $t = t_s > 0$, that generally depends on the guidance level w . Whether this occurs, the distortion variables when $t \leq t_s$ will read

$$\delta_\mu(t) = \frac{\sigma^2 + t}{\sigma^2 + t_s} \frac{(\sigma^2 + t_s)^{1+w}}{(\sigma^2 + t_s + 1)^w} \left[\left(1 + \frac{1}{\sigma^2 + t_s} \right)^{1+w} - 1 \right] + \frac{t_s - t}{\sigma^2 + t_s} - 1, \quad (138)$$

$$\delta_{\sigma^2}(t) = \frac{1}{\sigma^2 + t} \left[\left(\frac{\sigma^2 + t}{\sigma^2 + t_s} \right)^2 \frac{(\sigma^2 + t_s)^{2w+2}}{(\sigma^2 + t_s + 1)^{2w}} \frac{1}{2w+1} \left[\left(1 + \frac{1}{\sigma^2 + t_s} \right)^{2w+1} - 1 \right] + (t_s - t) \left(\frac{\sigma^2 + t}{\sigma^2 + t_s} \right) - (\sigma^2 + t) \right]. \quad (139)$$

Figure 8 represents the distortion estimators as evolving in time for a given realization of the control parameters: the two observables keep on decreasing in time. Figure 9 reports the entity of the distortion at sampling time $t = 0$, as well as the magnitude of the speciation time t_s for different combinations of the parameters. Generally speaking, large speciation times imply small distortion, and viceversa. Interestingly, the speciation time increases with the guidance level w , as guidance would reduce the distortion effects when w is very high. In fact, as also showed by Figures 10 and 6, the trend of $\delta_{\sigma^2}(0)$ presents a minimum at a given value of w and then increases. Also $\delta_\mu(0)$, according to our analytical computations, must decrease after reaching a maximum, that can be found at large values of w .

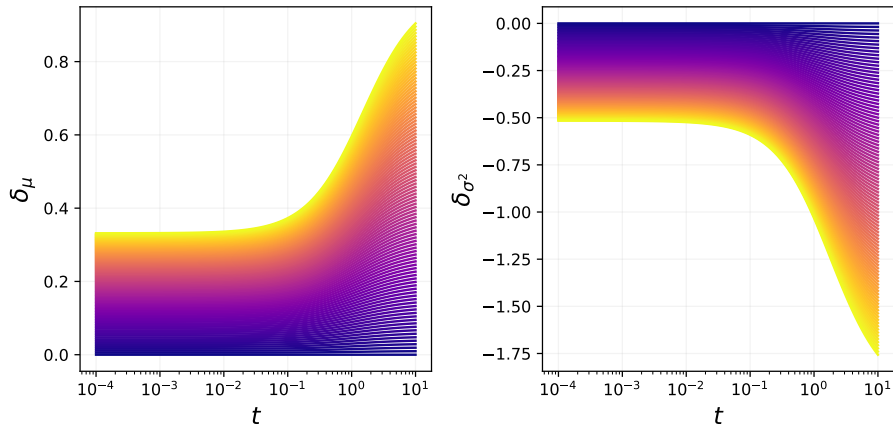


Figure 8. Distortion observables for a choice of σ^2, β that do not allow for the transition from the guided to the conditional phases of the potential. The system ends its run inside the guided phase. The color-map for the curves indicates different values of the guidance level: the darkest curve indicates $w = 0$, the lightest one $w = 1$.

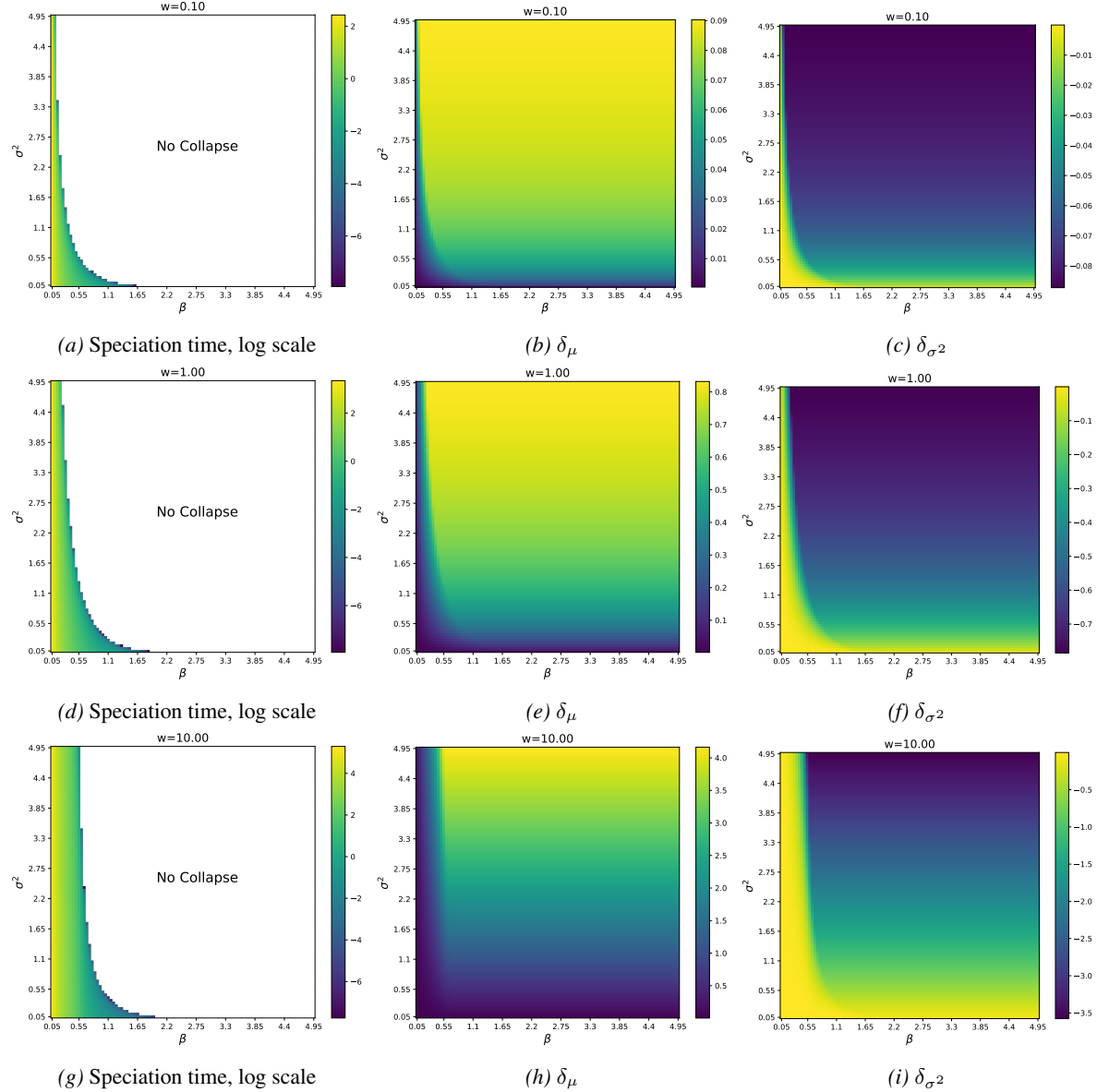


Figure 9. Heat-maps representing the distortion at $t = 0$ for various combinations of σ^2, β, w when the target distribution is a mixture of Gaussians with an exponential mode count. The blank region in the speciation time panel indicates $t_s < 0$, i.e. no transition from the guided to the conditional phase.

D. CFG prescriptions: time-dependent guidance level

Let us now evaluate different CFG prescription obtained through changing the guidance level w in time. Generally speaking we will solve our model by considering $w = w(t)$.

D.1. The goal of CFG

From our mean-field analysis of the guided diffusion potential we could conclude that, inside the guided phase, any $w \geq 0$ caused an expansion of the conditional mean, as well as a shrinkage of the variance.

Previous studies of CFG underline how this technique can be used to reach a favorable sampling condition where:

- Class-related means are more separated from each other, implying a better class separation.

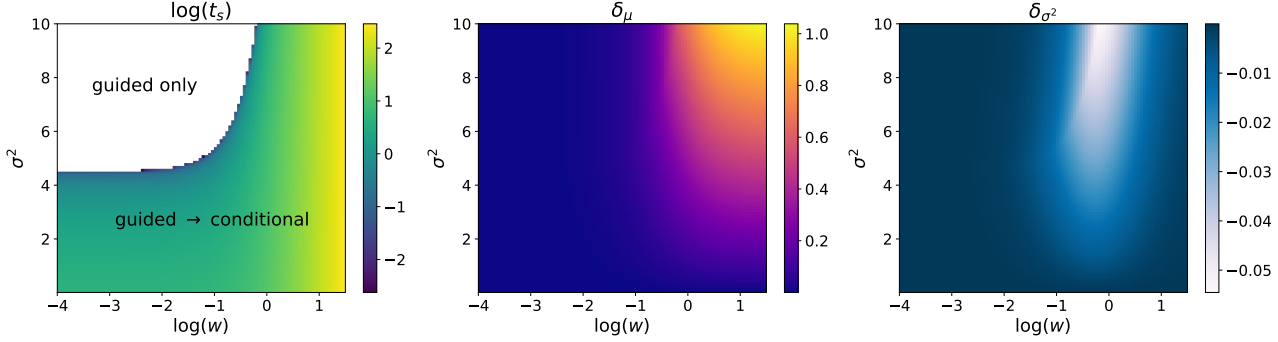


Figure 10. Measure of the speciation time t_s and the distortion estimators in the exponential regime as a functions of the control parameters σ^2 and w , for $\beta = 0.1$ at sampling time $t = 0$. The white region in the t_s panels signal that a negative speciation time, or equivalently, the absence of transition to the conditional phase. While this aspect is correlated to a stronger deformation of the target distribution, the occurrence of such transition appears to imply with a weak deformation, as testified by the behavior of δ_μ and δ_{σ^2} .

- The variance of sampled examples inside each class is not too small, to avoid loss of sample diversity.

Usually, for a given training dataset, reaching such condition requires a lot of empirical trials, and so far a theoretical criterion is lacking.

In the following sections we are going to analytically evaluate two different CFG prescriptions, namely:

- *Early-high*: w is high at large backward diffusion times, and low near sampling.
- *Early-low*: w is low at large backward diffusion times, and high near sampling.

Our theory suggests that, when $w < 0$, which is a peculiar choice in actual CFG, would imply an opposite trend: a shrinkage of the conditional mean and an expansion of the conditional variance (see Eqs. (33) and (34) from the main text). We hence suggest the simple following guidance prescription

$$w(t) = w_0 + \omega \cdot t, \quad w_0 \geq -1, \quad \omega > 0, \quad (140)$$

that allows to have a contrallable time window where the guidance level can be negative, boosting sample diversity. Let us analyze the effect of such prescription under the lens of tour theory, both in the case of *continuous classes* (see Section 4.1 and Appendix A) and *separated classes* (see Section 4.2 and Appendix B).

D.2. Multivariate Gaussian with Continuous Classes

Let us consider, as data distribution, the d -dimensional multivariate Gaussian introduced and analyzed in Appendix A. The matrix kernel that solves the backward SDE for this new guidance prescription reads

$$M(t_1, t_2) = e^{\int_{t_1}^{t_2} A(t') dt'}, \quad (141)$$

with

$$\int_{t_1}^{t_2} A(t) dt = \int_{t_1}^{t_2} \left[-(1 + w_0 + \omega t)(\Sigma_{x|c}^t)^{-1} + (w_0 + \omega t)(\Sigma_{xx}^t)^{-1} \right] dt = \int_{t_1}^{t_2} \left[-\frac{1 + w_0 + \omega t}{\Sigma_{x|c} + tI_{d_2}} + \frac{w_0 + \omega t}{\Sigma_{xx} + tI_{d_2}} \right] dt \quad (142)$$

$$= (\omega \Sigma_{x|c} - (1 + w_0)I_{d_2}) \log \left[\frac{\Sigma_{x|c} + t_2 I_{d_2}}{\Sigma_{x|c} + t_1 I_{d_2}} \right] - (\omega \Sigma_{xx} - w_0 I_{d_2}) \log \left[\frac{\Sigma_{xx} + t_2 I_{d_2}}{\Sigma_{xx} + t_1 I_{d_2}} \right], \quad (143)$$

Since we assumed that Σ_{xx} and $\Sigma_{x|c}$ commute, we can rewrite the matrix kernel as

$$M(t_1, t_2) = Z(t_1)Z(t_2)^{-1} \quad (144)$$

$$Z(t) = (\Sigma_{x|c} + tI_{d_2})^{(1+w_0)I_{d_2} - \omega \Sigma_{x|c}} (\Sigma_{xx} + tI_{d_2})^{-(w_0 I_{d_2} - \omega \Sigma_{xx})}, \quad (145)$$

and we are allowed to substitute matrices with the relative eigenvalues to compute integrals. More in the specific, one computes

$$\boldsymbol{\mu}_w(t) = \int_t^{+\infty} M(t, t') B(t') \boldsymbol{\mu} dt' = Z(t) \int_t^{+\infty} Z^{-1}(t') B(t') \boldsymbol{\mu} dt', \quad B(t) = (1+w_0+\omega t) (\Sigma_{x|c} + t I_{d_2})^{-1}, \quad (146)$$

$$\Sigma_w(t) = \int_t^{+\infty} M^2(t, t') dt' = Z^2(t) \int_t^{+\infty} Z^{-2}(t') dt'. \quad (147)$$

Call $R = \Sigma_{xx}$ and $S = \Sigma_{x|c}$ with eigenvalues (r_i, s_i) , then

$$\boldsymbol{\mu}_w(t) = P \operatorname{diag}(\lambda_1(t), \dots, \lambda_{d_2}(t)) P^{-1}, \quad (148)$$

where P is the unitary matrix collecting the common eigenvectors to R and S and

$$\lambda_i(t) = \frac{(s_i + t)^{(1+w_0)-\omega s_i}}{(r_i + t)^{w_0-\omega r_i}} \left[\int_t^{+\infty} \left(\frac{s_i + t'}{r_i + t'} \right)^{-w_0} \frac{(s_i + t')^{\omega s_i - 2}}{(r_i + t')^{\omega r_i}} (1 + w_0 + \omega t') dt' \right], \quad (149)$$

that I can re-write in terms of incomplete Beta functions as

$$\begin{aligned} \lambda_i(t) = & \frac{(s_i + t)^{(1+w_0)-\omega s_i}}{(r_i + t)^{w_0-\omega r_i}} (r_i - s_i)^{-\omega(r_i - s_i) - 1} \left[(1 + w_0 - \omega s_i) \times \right. \\ & \times \left(B_1(\omega s_i - w_0 - 1, \omega(r_i - s_i)) - B_{\frac{s_i+t}{r_i+t}}(\omega s_i - w_0 - 1, \omega(r_i - s_i)) \right) + (\omega r_i - (1 + w_0)) \times \\ & \times \left. \left(B_1(\omega s_i - w_0, \omega(r_i - s_i)) - B_{\frac{s_i+t}{r_i+t}}(\omega s_i - w_0, \omega(r_i - s_i)) \right) \right]. \end{aligned} \quad (150)$$

where the incomplete Beta function $B_f(a, b)$ is defined as

$$B_f(a, b) = \int_0^f dr r^{a-1} (1-r)^{b-1}, \quad (151)$$

Beta functions are easy to compute numerically. At the same way, the covariance matrix reads

$$\Sigma_w(t) = P \operatorname{diag}(e_1(t), \dots, e_{d_2}(t)) P^{-1}, \quad (152)$$

where

$$e_i(t) = (s_i + t) \cdot \Lambda_i(t), \quad (153)$$

with

$$\Lambda_i(t) = (s_i + t)^{1+2(w_0-\omega s_i)} (r_i + t)^{-2w_0+2\omega r_i} \int_t^{+\infty} \left(\frac{s_i + t'}{r_i + t'} \right)^{-2w_0} \left[\frac{(s_i + t')^{s_i}}{(r_i + t')^{r_i}} \right]^{2\omega} \frac{dt'}{(s_i + t')^2}, \quad (154)$$

which can be expressed in terms of incomplete Beta functions as

$$\begin{aligned} \Lambda_i(t) = & (s_i + t)^{1+2(w_0-\omega s_i)} (r_i + t)^{-2w_0+2\omega r_i} (r_i - s_i)^{-2\omega(r_i - s_i) - 1} \times \\ & \times \left[B_1(2(\omega s_i - w_0) - 1, 2\omega(r_i - s_i) + 1) - B_{\frac{s_i+t}{r_i+t}}(2(\omega s_i - w_0) - 1, 2\omega(r_i - s_i) + 1) \right]. \end{aligned} \quad (155)$$

Let us consider one direction i of the ambient space and one choice of the eigenvalues of Σ_{xx} and $\Sigma_{x|c}$, respectively $r_i = 1$ and $s_i = 0.6$. At this point we can trace a phase-diagram of distortion as a function of w_0 and ω , that is represented in Figure 11a. We identify one region where we have $\lambda > 1$ and $\Lambda > 1$ simultaneously, and it occurs when $w_0 < 0$ and ω is smaller than a characteristic value which depends on the data distribution. Outside this region, the width of the negative-guidance window is not large enough to improve sample diversity and allow $\Lambda > 1$. We also simulated the system for one choice of the class and covariance matrices at different values of w_0 and ω . As we can notice from Figure 11b there is a little improvement of the performance, that becomes more evident when the time window is larger, i.e. when w_0 is largely negative and ω is small. As showed in Figure 12, we find that for this class of data distributions the effects of the schedule must be mild, since we need a large difference between the eigenvalues $r_i - s_i$ to achieve significant expansions of the covariances, and this might not occur along all the directions of the data space.

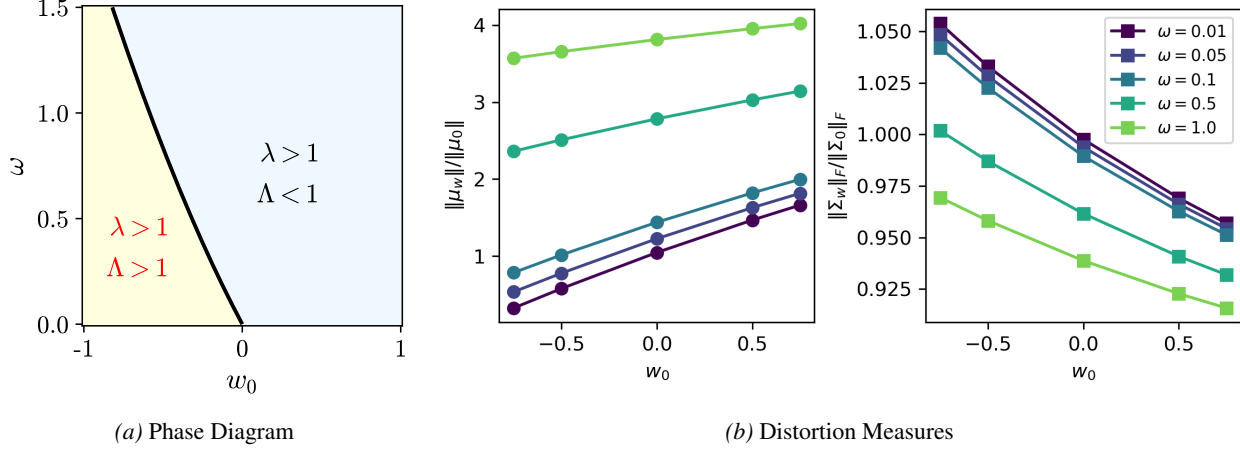


Figure 11. The effect of linear early-high CFG schedules where the guidance level is allowed to become negative on a multivariate Gaussian target, depending on two parameters w_0 and ω . Panel (a) represents a phase diagram for $r = 1, s = 0.6$. The beneficial region is in yellow: here both distortion weights are larger than unity. The outer region contains schedules where the mean is expanded and covariances are contracted. Panel (b) reports distortion estimators at $t = 0$ measured from numerical simulations at different values of w_0 and ω , for $d_1 = 1$ and $d_2 = 9$. Specifically: the norm of the mean divided by the norm of the conditional mean on the left; the norm of the covariance matrix divided by the norm of the conditional covariance matrix on the right. As we can notice, for small values of w_0 and small values of ω (i.e. a large negative guidance time window) we reach the yellow region of the phase diagram. The general effect is mild with this target distribution, because positive distortion is enhanced only along directions where the difference $r_i - s_i$ is large.

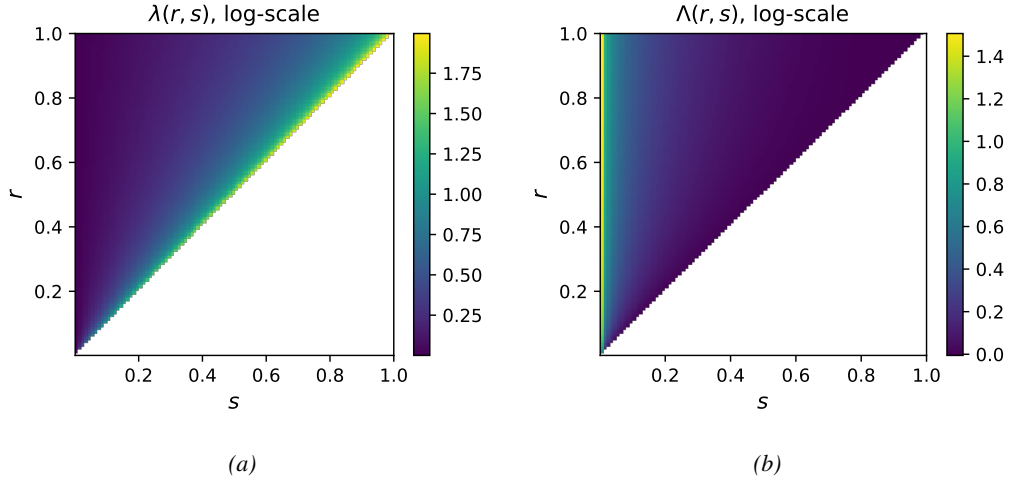


Figure 12. Distortion weights λ and Λ as functions of the eigenvalues $(r, s) \in [0, 1]^2$, with $s \leq r$, for a linear early-high CFG schedule with $w_0 = -0.75$ and $\omega = 1$. The values are plotted in log-scale for enhancement. Panel (a) shows that the mean is expanded significantly only when $s_i \simeq r_i$. Panel (b) displays a significant distortion of covariances in the opposite case, i.e. $r_i - s_i$ large. This behavior implies that the effects of such CFG prescription must be mild in general.

D.3. Mixture of an Exponential number of Gaussians

Let us consider a target distribution being a mixture of M Gaussians where $M = e^{\beta d}$ and centroids are d -dimensional normal vectors. Then the REM theory developed in Appendix B applies and the backward SDE is

$$dx = x \frac{\sigma^2 + t + 1 + w_0 + \omega t}{(\sigma^2 + t)(\sigma^2 + t + 1)} dt - c^1 \frac{1 + w_0 + \omega t}{(\sigma^2 + t)} dt + dW_t \quad (156)$$

The auxiliary functions read

$$a(t) = \frac{\sigma^2 + t + 1 + w_0 + \omega t}{(\sigma^2 + t)(\sigma^2 + t + 1)}, \quad b(t) = -c^1 \frac{1 + w_0 + \omega t}{\sigma^2 + t}, \quad (157)$$

$$\Phi(t) = \left(\frac{\sigma^2}{\sigma^2 + t} \right)^{1+w_0-\omega\sigma^2} \left(\frac{1+\sigma^2}{\sigma^2 + t + 1} \right)^{\omega(1+\sigma^2)-w_0}. \quad (158)$$

The evolution equation reads

$$x_t = \left(\frac{\sigma^2 + t}{\sigma^2 + T} \right)^{1+w_0-\omega\sigma^2} \left(\frac{\sigma^2 + t + 1}{\sigma^2 + T + 1} \right)^{\omega(1+\sigma^2)-w_0} x_T - c^1 \frac{(\sigma^2 + t)^{1+w_0-\omega\sigma^2}}{(\sigma^2 + t + 1)^{w_0-\omega(1+\sigma^2)}} \quad (159)$$

$$\times \left[(1 + w_0 - \omega\sigma^2) [B_{f(t)}(\omega\sigma^2 - w_0 - 1, \omega) - B_{f(T)}(\omega\sigma^2 - w_0 - 1, \omega)] \right. \quad (160)$$

$$\left. + (\omega(1 + \sigma^2) - w_0 - 1) [B_{f(t)}(\omega\sigma^2 - w_0, \omega) - B_{f(T)}(\omega\sigma^2 - w_0, \omega)] \right] \quad (161)$$

$$+ \frac{(\sigma^2 + t)^{1+w_0-\omega\sigma^2}}{(\sigma^2 + t + 1)^{w_0-\omega(1+\sigma^2)}} \int_T^t ds \xi(s) \frac{(\sigma^2 + s + 1)^{w_0-\omega(1+\sigma^2)}}{(\sigma^2 + s)^{1+w_0-\omega\sigma^2}}, \quad (162)$$

where the incomplete Beta function $B_f(a, b)$ are defined in Eq. (151) and the function $f(x)$ appearing in our version of the Beta function reads

$$f(x) = \frac{\sigma^2 + x}{\sigma^2 + x + 1}. \quad (163)$$

Incomplete Beta functions are easy to compute numerically. Instead, x_t is the initial condition for the integration. From the isotropy of the process, the solution x_t must be normally distributed with mean

$$\mu(t) = \left(\frac{\sigma^2 + t}{\sigma^2 + T} \right)^{1+w_0-\omega\sigma^2} \left(\frac{\sigma^2 + t + 1}{\sigma^2 + T + 1} \right)^{\omega(1+\sigma^2)-w_0} \mu(T) - c^1 \frac{(\sigma^2 + t)^{1+w_0-\omega\sigma^2}}{(\sigma^2 + t + 1)^{w_0-\omega(1+\sigma^2)}} \quad (164)$$

$$\times \left[(1 + w_0 - \omega\sigma^2) [B_{f(t)}(\omega\sigma^2 - w_0 - 1, \omega) - B_{f(T)}(\omega\sigma^2 - w_0 - 1, \omega)] \right. \quad (165)$$

$$\left. + (\omega(1 + \sigma^2) - w_0 - 1) [B_{f(t)}(\omega\sigma^2 - w_0, \omega) - B_{f(T)}(\omega\sigma^2 - w_0, \omega)] \right] \quad (166)$$

and variance

$$\sigma^2(t) = \left(\frac{\sigma^2 + t}{\sigma^2 + T} \right)^{2(1+w_0-\omega\sigma^2)} \left(\frac{\sigma^2 + t + 1}{\sigma^2 + T + 1} \right)^{2\omega(1+\sigma^2)-2w_0} \sigma^2(T) \quad (167)$$

$$+ \frac{(\sigma^2 + t)^{2(1+w_0-\omega\sigma^2)}}{(\sigma^2 + t + 1)^{2w_0-2\omega(1+\sigma^2)}} [B_{f(t)}(2\omega\sigma^2 - 2w_0 - 1, 1 + 2\omega) - B_{f(T)}(2\omega\sigma^2 - 2w_0 - 1, 1 + 2\omega)]. \quad (168)$$

An initial condition $\sigma^2(T) = \mathcal{O}(T)$ should require $w > -1/2$, that is always satisfied in this case. At this point one can perform the $T \rightarrow \infty$ obtaining

$$\mu(t) = -c^1 \frac{(\sigma^2 + t)^{1+w_0-\omega\sigma^2}}{(\sigma^2 + t + 1)^{w_0-\omega(1+\sigma^2)}} \quad (169)$$

$$\times \left[(1 + w_0 - \omega\sigma^2) [B_{f(t)}(\omega\sigma^2 - w_0 - 1, \omega) - B_1(\omega\sigma^2 - w_0 - 1, \omega)] \right. \quad (170)$$

$$\left. + (\omega(1 + \sigma^2) - w_0 - 1) [B_{f(t)}(\omega\sigma^2 - w_0, \omega) - B_1(\omega\sigma^2 - w_0, \omega)] \right], \quad (171)$$

$$\sigma^2(t) = \frac{(\sigma^2 + t)^{2(1+w_0-\omega\sigma^2)}}{(\sigma^2 + t + 1)^{2w_0-2\omega(1+\sigma^2)}} [B_{f(t)}(2\omega\sigma^2 - 2w_0 - 1, 1 + 2\omega) - B_1(2\omega\sigma^2 - 2w_0 - 1, 1 + 2\omega)]. \quad (172)$$

At this point the distortion estimators become

$$\delta_\mu(t) = -\frac{(\sigma^2 + t)^{1+w_0-\omega\sigma^2}}{(\sigma^2 + t + 1)^{w_0-\omega(1+\sigma^2)}} \quad (173)$$

$$\times \left[(1 + w_0 - \omega\sigma^2) [B_{f(t)}(w\sigma^2 - w_0 - 1, \omega) - B_1(\omega\sigma^2 - w_0 - 1, \omega)] \right. \quad (174)$$

$$\left. + (\omega(1 + \sigma^2) - w_0 - 1) [B_{f(t)}(\omega\sigma^2 - w_0, \omega) - B_1(\omega\sigma^2 - w_0, \omega)] \right] - 1, \quad (175)$$

and

$$\delta_{\sigma^2}(t) = \frac{1}{\sigma^2 + t} \left(\frac{(\sigma^2 + t)^{2(1+w_0-\omega\sigma^2)}}{(\sigma^2 + t + 1)^{2w_0-2\omega(1+\sigma^2)}} [B_{f(t)}(2\omega\sigma^2 - 2w_0 - 1, 1 + 2\omega) - B_1(2\omega\sigma^2 - 2w_0 - 1, 1 + 2\omega)] - \sigma^2 - t \right), \quad (176)$$

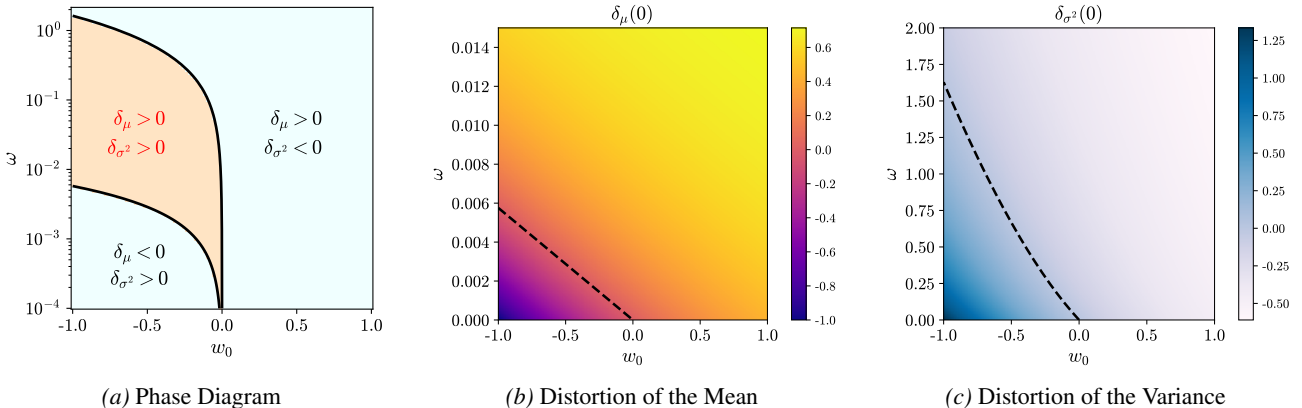


Figure 13. The effect of linear late-high CFG schedule where the guidance level is allowed to become negative, depending on two parameters w_0 and ω . The variance of the mode is $\sigma^2 = 0.75$ and the mode density β has been chosen to be large, so that the system never enters the conditional phase in the displayed domain. The first panel from the left is a phase diagram reporting the beneficial region in orange: here both means and variances are enlarged. The other regions either show loss of separability or tendency to shrink the mode variance. The following panels report distortion estimators. Dashed lines signal the passage from a negative distortion at time $t = 0$, to a positive one.

Sanity check: a guidance prescription that is solvable in closed form

Let us consider a late-high linear prescription where $w_0 = \sigma^2 - 1$ and $\omega = 1$. Then one has

$$w(t) = \sigma^2 + t - 1. \quad (177)$$

The guidance level can become negative at $t^* = 1 - \sigma^2$, whether $\sigma^2 < 1$. This choice for $w(t)$ simplifies the SDE per component of the guided phase of the potential into

$$dx = \frac{2x}{\sigma^2 + t + 1} dt - c^1 dt + dW_t. \quad (178)$$

The auxiliary functions read

$$a(t) = \frac{w}{\sigma^2 + t}, \quad b(t) = -c^1, \quad \Phi(t) = \left(\frac{\sigma^2 + 1}{\sigma^2 + t + 1} \right)^2. \quad (179)$$

The evolution equation reads

$$x_t = \left(\frac{\sigma^2 + t + 1}{\sigma^2 + T + 1} \right)^2 x_T + \left[(\sigma^2 + t + 1) - \frac{(\sigma^2 + t + 1)^2}{\sigma^2 + T + 1} \right] c^1 + (\sigma^2 + t + 1)^2 \int_T^t ds \frac{\xi(s)}{(\sigma^2 + s + 1)^2}, \quad (180)$$

where x_t is the initial condition for the integration. From the isotropy of the process, the solution x_t must be normally distributed with mean

$$\mu(t) = \left(\frac{\sigma^2 + t + 1}{\sigma^2 + T + 1} \right)^2 \mu(T) + \left[(\sigma^2 + t + 1) - \frac{(\sigma^2 + t + 1)^2}{\sigma^2 + T + 1} \right] c^1, \quad (181)$$

and variance

$$\sigma^2(t) = \left(\frac{\sigma^2 + t + 1}{\sigma^2 + T + 1} \right)^4 \sigma^2(T) + \frac{(\sigma^2 + t + 1)^4}{3} \left[\frac{1}{(\sigma^2 + t + 1)^3} - \frac{1}{(\sigma^2 + T + 1)^3} \right]. \quad (182)$$

When $T \gg 1$ the same moments become

$$\mu(t) = (\sigma^2 + t + 1) c^1, \quad (183)$$

$$\sigma^2(t) = \frac{(\sigma^2 + t + 1)}{3}. \quad (184)$$

As a consequence, the deformation observable evolve in time according to

$$\delta_\mu(t) = \sigma^2 + t, \quad (185)$$

$$\delta_{\sigma^2}(t) = \frac{1}{3\sigma^2} (t + 1 - 2\sigma^2). \quad (186)$$

If we choose $\sigma^2 \leq 1/2$ we can obtain the desired condition $\delta_\mu(0) = \sigma^2 > 0$ and $\delta_{\sigma^2}(0) = \frac{1-2\sigma^2}{3} \geq 0$. In this setup, we can still have collapse of the potential to the phase where its local minimum is centered on c^1 . In this phase the diffusion potential is centered on the class, so diffusion will be drifted towards a situation where $\delta_\mu > 0$ and $\delta_{\sigma^2} < 0$. This transition occurs when the collapse time t_s satisfies the following condition

$$t_s = \frac{1}{e^{2\beta-1} - 1} - \sigma^2 > 0, \quad \beta > 1/2. \quad (187)$$

Specifically, when $\beta \rightarrow 1/2$ we have $t_s \rightarrow \infty$, implying zero distortion of the target measure, regardless of the value of σ^2 . When $\beta \leq 1/2$ the REM free-energy of the model is strictly negative implying the system to always live in the conditional phase, implying no distortion.

E. Additional experimental results

In this Section we provide additional results about the experiments described in Sec. 3. We generate a dataset of images from Stable Diffusion (v1.5) (Rombach et al., 2022): for 50 different prompts we generate 20 images at different guidance levels. For each prompt and guidance level samples are then mean-centered, and we measure metrics in pixel space, reported in Fig. 15, as well as in feature space, Fig. 14, using both CLIP and DINOv2 embeddings.

Pixel-level metrics (pixel variance, L_2 distance to the group mean) show a non-monotonic dependence on guidance. Variability decreases from low to intermediate guidance values, indicating suppression of stochastic noise and fine-scale variation, but increases again at high guidance. This rebound coincides with increasing structural similarity (SSIM) and is consistent with the emergence of sharpening and saturation artifacts rather than meaningful diversity. Principal component analysis (PCA) in pixel space reveals a monotonic increase in the explained variance of the first principal component and a corresponding decrease in participation ratio, indicating that pixel-space variability becomes progressively low-rank as guidance increases. However, pixel-space PCA conflates semantic variation with texture and artifact-level effects, limiting interpretability. Perceptual similarity measured by LPIPS exhibits a weaker and less consistent dependence on guidance in pixel space. While LPIPS generally decreases with increasing guidance, indicating reduced perceptual variability, the trend is comparatively shallow, suggesting that pixel-space LPIPS remains partially sensitive to high-guidance artifacts and local texture changes, and therefore does not fully disentangle perceptual collapse from artifact-driven effects.

In contrast, feature-space analysis exhibits clear and monotonic trends. Both CLIP and DINOv2 feature variance, L_2 distance to the mean, and cosine distance to the mean decrease steadily with increasing guidance, without the high-guidance rebound observed in pixel space. This indicates a genuine reduction of perceptual and semantic diversity rather than artifact-driven effects. DINOv2 features show a faster initial reduction in variability than CLIP features, suggesting that guidance first

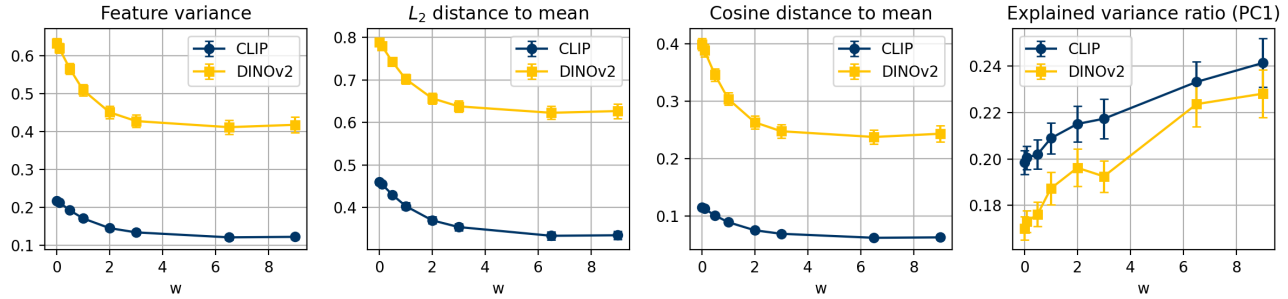


Figure 14. Variance metrics in feature space.

suppresses structural and layout-level variation. CLIP features collapse more strongly at higher guidance values, indicating a subsequent reduction in semantic diversity. This ordering is further supported by PCA geometry: the participation ratio decreases monotonically in both spaces, but remains consistently higher for DINOv2 than for CLIP, while the explained variance of the first principal component grows more strongly in CLIP space.

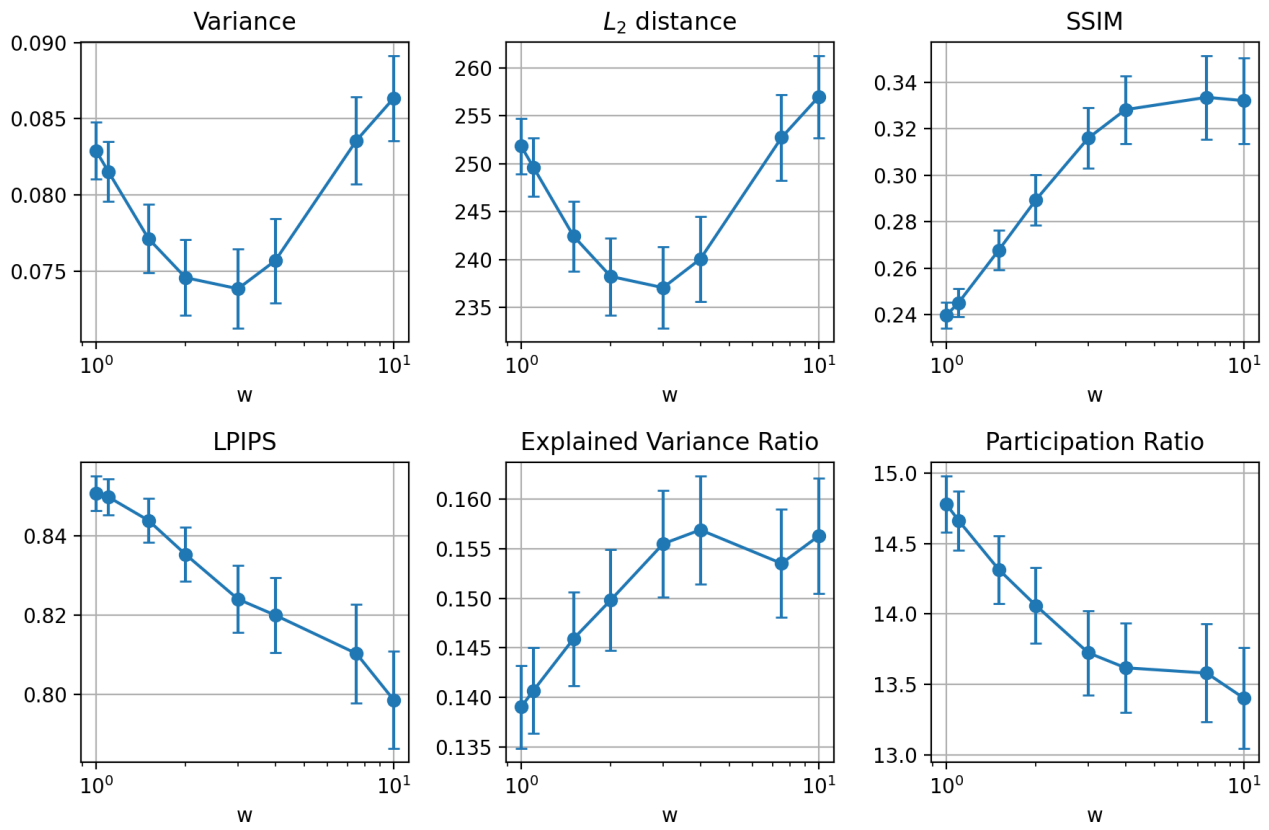


Figure 15. Variance metrics in pixel space.

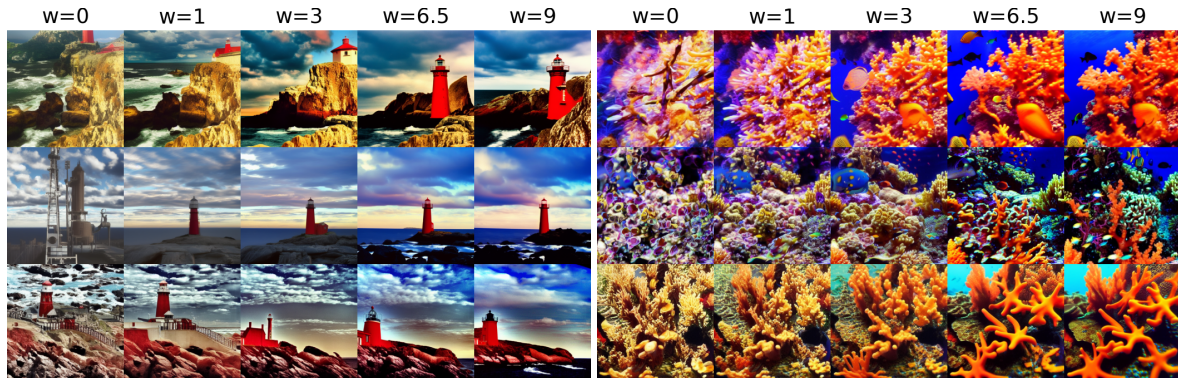


Figure 16. Samples of images generated with Stable Diffusion v1.5 at different guidance levels. Rows are different random seeds, columns refer to guidance levels.